

# JGR Solid Earth

## RESEARCH ARTICLE

10.1029/2024JB029487

### Key Points:

- Natural fractures significantly impact fracture initiation, propagation, and connectivity evolution during hydraulic fracturing
- Low-strength fractures break due to altered in-situ stress, resulting in the final fracture networks forming a multi-cluster system
- Heterogeneity is crucial in forming final fracture networks, and high injection rates and viscosity exacerbate their influence areas

### Supporting Information:

Supporting Information may be found in the online version of this article.

### Correspondence to:

M. Wang and S. Qi,  
mrwang@tsinghua.edu.cn;  
qishengwen@mail.iggcas.ac.cn

### Citation:

Zhu, W., Chen, Z., He, X., Liu, J., Guo, S., Zheng, B., et al. (2024). Numerical analysis of the dynamic mechanisms in hydraulic fracturing with a focus on natural fractures. *Journal of Geophysical Research: Solid Earth*, 129, e2024JB029487. <https://doi.org/10.1029/2024JB029487>

Received 8 MAY 2024

Accepted 25 NOV 2024

### Author Contributions:

**Conceptualization:** Weiwei Zhu, Xupeng He, Ali Yousef, Shengwen Qi, Moran Wang

**Data curation:** Weiwei Zhu

**Formal analysis:** Weiwei Zhu, Zhiqiang Chen, Xupeng He, Jingyao Liu, Songfeng Guo, Bowen Zheng, Ali Yousef, Shengwen Qi, Moran Wang

**Funding acquisition:** Shengwen Qi, Moran Wang

**Investigation:** Weiwei Zhu, Zhiqiang Chen, Xupeng He, Jingyao Liu, Songfeng Guo, Bowen Zheng, Ali Yousef, Shengwen Qi, Moran Wang







**Methodology:** Weiwei Zhu, Zhiqiang Chen, Bowen Zheng, Shengwen Qi, Moran Wang

**Project administration:** Moran Wang

**Resources:** Zhiqiang Chen, Ali Yousef

**Software:** Weiwei Zhu, Zhiqiang Chen

## Numerical Analysis of the Dynamic Mechanisms in Hydraulic Fracturing With a Focus on Natural Fractures

Weiwei Zhu<sup>1,2,3</sup> , Zhiqiang Chen<sup>4</sup>, Xupeng He<sup>5</sup> , Jingyao Liu<sup>6</sup>, Songfeng Guo<sup>1,2</sup> , Bowen Zheng<sup>1,2</sup>, Ali Yousef<sup>5</sup>, Shengwen Qi<sup>1,2</sup>  , and Moran Wang<sup>3</sup> 

<sup>1</sup>State Key Laboratory of Lithospheric and Environmental Coevolution, Institute of Geology and Geophysics, Chinese Academy of Sciences, Beijing, China, <sup>2</sup>College of Earth and Planetary Sciences, University of Chinese Academy of Sciences, Beijing, China, <sup>3</sup>Department of Engineering Mechanics, Tsinghua University, Beijing, China, <sup>4</sup>Petroleum Exploration and Production Research Institute, SINOPEC, Beijing, China, <sup>5</sup>EXPEC Advanced Research Center, Saudi Aramco, Dhahran, Kingdom of Saudi Arabia, <sup>6</sup>Research Institute of Petroleum Exploration & Development, China National Petroleum Corporation, Beijing, China

**Abstract** The hydraulic fracturing process is a prominent example of fracture network evolution under stress. However, the interactions between hydraulic fractures and natural fracture networks, along with the connectivity evolution of the resultant fracture networks, require more research. This research incorporates discrete fracture networks to characterize subsurface structures and employs the Discrete Element - Lattice Boltzmann Method to simulate the hydraulic fracturing process. The dynamic evolution of subsurface structures, including the initiation of hydraulic fractures and their interaction with natural fractures, is systematically investigated. Results indicate that natural fractures significantly impact fracture initiation, propagation, and connectivity evolution, which in turn affects fluid production. Fracture strength is key for the interaction, and hydraulic fractures tend to propagate along weak natural fractures with low resistance. Fracture strength variability determines the final fracture networks, with low-strength fractures breaking due to the altered in-situ stress and forming local clusters. High injection rates and fluid viscosity result in a large pressure buildup and exaggerate the influential region. A multi-cluster system is thus formed during the hydraulic fracturing process, and its connectivity can be well quantified with a novel connectivity metric. In low-permeable reservoirs, fracture clusters connected to production wells can contribute instantly, while local clusters may contribute to production from a long-term perspective. Injection rate, fluid viscosity, fracture orientation, and clustering effects have consistent positive correlations with the total connectivity and production. Heterogeneity has a weak positive correlation with fluid production, while a moderate negative correlation with total connectivity.

**Plain Language Summary** Hydraulic fracturing is a widely employed technique in developing unconventional reservoirs. Ubiquitous natural fractures in the deep subsurface significantly influence the hydraulic fracturing outcomes; however, the interactions between hydraulic and natural fractures remain incompletely understood. In this work, we optimize the numerical scheme to incorporate natural fractures and explore their impact on hydraulic fracturing. We found that natural fractures significantly impact fracture initiation, propagation, and connectivity evolution, which in turn affects fluid production. Fracture strength is key for the interaction, and hydraulic fractures tend to propagate along weak natural fractures with low resistance. Fracture strength variability can significantly impact the final fracture networks. Low-strength fractures tend to break due to the altered in-situ stress, forming local clusters. High injection rates and fluid viscosity result in a large pressure buildup and exaggerate the influential region. Furthermore, we propose a connectivity metric to quantify the connectivity evolution of multi-cluster fracture networks formed during the hydraulic fracturing process. Therefore, the quantitative analysis of sensitivity for influential factors on connectivity and production is available and discussed. These findings are essential for us to better understand the subsurface structures and their dynamic evolution under the hydraulic fracturing process.

## 1. Introduction

Fractures are fundamental subsurface features that introduce significant heterogeneity to geological structures and play a crucial role in controlling the mechanical and hydrological properties of rock masses (Qi et al., 2004; Zhu et al., 2021; Zoback & Gorelick, 2012). Characterizing subsurface fracture networks and investigating their

**Supervision:** Shengwen Qi, Moran Wang

**Validation:** Weiwei Zhu, Xupeng He, Bowen Zheng, Moran Wang

**Writing – original draft:** Weiwei Zhu, Zhiqiang Chen, Xupeng He, Jingyao Liu, Songfeng Guo, Bowen Zheng, Moran Wang

**Writing – review & editing:** Ali Yousef, Shengwen Qi, Moran Wang

dynamic evolution under stress disturbances represent critical challenges in geoscience (Gabriel et al., 2024; Zhu, Khirevich, & Patzek, 2022).

A prominent example of fracture network evolution under stress is hydraulic fracturing, a technique widely applied in unconventional reservoirs—such as shale gas, shale oil, and coalbed methane—to enhance resource recovery (Gandossi & Von Estorff, 2013; Marsden et al., 2022; Pruess, 2006). Additionally, hydraulic fracturing provides valuable insights into the subsurface environment, such as enabling the measurement of in-situ stress states (Haimson & Fairhurst, 1969; Lakirouhani et al., 2016; Zoback & Haimson, 1982). Hydraulic fracturing creates complex, high-permeability fracture networks in low-permeability formations, which include both artificial fractures and reactivated natural fractures (Rateman et al., 2018; Zhu, He, Khirevich, & Patzek, 2022). This complex fracture network is referred to as the stimulated reservoir volume (H. Chen et al., 2018; Fisher et al., 2002; Mayerhofer et al., 2010), which is key to evaluating the performance of hydraulic fracturing operations. Understanding the mechanism of fracture propagation and network development during hydraulic fracturing is essential for advancing knowledge of fracture network evolution in subsurface environments. The insights gained are beneficial not only for various engineering applications but also for understanding environmental and geohazard processes, such as landslides or earthquakes (Gabriel et al., 2024; Qi et al., 2004), as fractures play a critical role in these phenomena. Consequently, many theoretical, experimental, and numerical studies have been conducted to deepen our understanding of the hydraulic fracturing process (Bing et al., 2014; Z. Chen, Jin, & Wang, 2018; Z. Chen, Yang, & Wang, 2018; Chuprakov et al., 2011; Geertsma & De Klerk, 1969; Khristianovic & Zheltov, 1955; Kolawole & Ispas, 2020; Kumari et al., 2018; Liu et al., 2018; Marder et al., 2015; Nordgren, 1972; Perkins & Kern, 1961; Taleghani & Olson, 2014).

Analytical models, such as the classic Perkins-Kern-Nordgren (PKN) model (Nordgren, 1972; Perkins & Kern, 1961) and the Kristianovich-Geertsma-de Klerk (KGD) model (Geertsma & De Klerk, 1969; Khristianovic & Zheltov, 1955), and extended analytical models (Marder et al., 2015), usually have significant simplifications in terms of fracture shapes and propagation process. They are useful for rough estimations in actual engineering applications, but insufficient for revealing the micro-mechanisms of hydraulic fracturing, especially when it comes to the complex interaction between hydraulic and natural fractures.

Lab experiments include the hydraulic fracturing process in natural rocks and artificial rocks. In the natural rocks, the impact of injection rate, fluid viscosity, and in-situ stress states can be examined, and the interaction between hydraulic fractures and the preexisting natural fractures can also be observed (Bing et al., 2014; Kumari et al., 2018; Liu et al., 2018). However, the natural fractures in rocks cannot be artificially designed, and systematic analysis of their impact on the hydraulic fracturing process is difficult. In the artificial rocks, pre-existing fractures can be well-designed and embedded in the rock. Olson et al. (2012) used glass slides to mimic natural fractures, which are embedded in the hydrostone. Furthermore, Bahorich et al. (2012) used sandstone slides, plaster slides, and glass slides to mimic sealed natural fractures with different strengths. Different interaction patterns, like bypassing, diverted along the natural fractures, arresting at the natural fractures, and a combination of bypassing and diversion, are well observed. However, artificial rocks (hydrostone or plaster) are different from actual rocks, and natural fractures with different cement materials and sealing patterns also exhibit heterogeneous strengths and form complex fracture networks (S. E. Laubach & Ward, 2006; Ukar & Laubach, 2016), making it challenging to incorporate those characteristics in the experiments.

Numerical simulations provide a practical approach to investigate fracture network evolution during the hydraulic fracturing process, considering the interaction between hydraulic fractures and natural fractures. Different numerical schemes are adopted to couple rock deformation and fluid flow to model the hydraulic fracturing process (Z. Chen & Wang, 2017; Krzaczek et al., 2021; Wang et al., 2024; Wu & Olson, 2016; Zhou et al., 2023). Many factors are found to affect the propagation of hydraulic fractures when encountering natural fractures, such as the mechanical properties of the natural fractures, the approaching angle between hydraulic and natural fractures, and differential stress (Z. Chen, Jin, & Wang, 2018; Z. Chen, Yang, & Wang, 2018; Chuprakov et al., 2011; Kolawole & Ispas, 2020; Taleghani & Olson, 2014). In Z. Chen, Yang, and Wang (2018)'s work, they concluded that the bond strength of natural fractures plays an essential role in controlling the interaction mode between hydraulic and natural fractures, and they provide a critical threshold ratio of 0.67 in homogeneous rocks.

In most numerical studies, pre-existing natural fractures are significantly simplified. Many works focus on the interaction between hydraulic fractures and a few natural fractures or regular fracture patterns, such as constant fracture lengths, uniformly distributed fracture centers, or single-oriented fracture sets (S. Li et al., 2017; Wang

et al., 2024; Wu & Olson, 2016; Yaobin et al., 2020; Zeng & Yao, 2016). However, natural fracture networks are much more complex. From outcrop observations and analyses, natural fracture networks often exhibit clustering phenomena, their lengths tend to follow a power-law distribution, and their orientations can be close to a uniform distribution (Zhu, He, Santoso, et al., 2022). These complexities should be properly accounted for when describing pre-existing fracture networks.

The Discrete Fracture Network (DFN) method was proposed to simulate complex subsurface structures with different statistical distributions describing key geometrical properties of fractures (Zhu, Khirevich, & Patzek, 2022; Lei et al., 2017). It provides an alternative approach to study subsurface structures using a stochastic method. For instance, Y. Li et al. (2021) incorporated the DFN model into the numerical simulation of hydraulic fracturing in a naturally fractured reservoir using the Displacement Discontinuity Method (DDM). However, it is challenging for DDM to investigate the complex fracture initiation and propagation processes. Therefore, a systematic investigation of the impact of natural fractures, coupled with other factors in the hydraulic fracturing process, is still lacking—particularly when considering the heterogeneous characteristics of natural fractures and complex fracture networks.

More importantly, the connectivity of the generated fracture network is essential for assessing the dynamic evolution of complex subsurface structures, as connectivity is intricately tied to the mechanical and hydrologic properties of the fracture network. Such investigations are rarely conducted because quantifying the connectivity of complex fracture networks is challenging, especially for multi-cluster fracture networks formed during the hydraulic fracturing process. From laboratory experiments, numerical simulations and field microseismicity observations, it is evident that local clusters are formed due to the altered in-situ stress (Liu et al., 2016; Riffault et al., 2018; Zhu et al., 2023). Traditional methods like percolation theory, connectivity field, geological entropy, and the ternary diagram and its extensions are not suitable for quantifying connectivity in such complex fracture networks (Alghalandis et al., 2015; C. Barton & Hsieh, 1989; Berkowitz et al., 2000; Bour & Davy, 1997; Sanderson & Nixon, 2015; Ye et al., 2021).

Therefore, to systematically investigate the dynamic evolution of fracture networks during the hydraulic fracturing process, three key technical issues must be addressed: the generation of a complex pre-existing natural fracture network, the incorporation of the pre-existing natural fracture network into the hydraulic fracturing simulation, and the quantification of connectivity and its evolution during the hydraulic fracturing process. Significant research has been conducted by the team, where an efficient DFN software, HATCHFRAC, has been developed to generate complex discrete fracture networks (Zhu, Khirevich, & Patzek, 2022). A DEM-LBM method has been proposed to simulate the hydraulic fracturing process, and the impact of individual factors has been systematically investigated, including in-situ stress, injection rate, fluid viscosity, rock strength heterogeneity, and permeability (Zhu et al., 2023). Additionally, a novel connectivity metric has been proposed to quantify the connectivity of complex fracture networks composed of multiple clusters and to investigate connectivity evolution during the fracturing process (Zhu et al., 2024). With all the previous groundwork in place, this investigation is now possible. Therefore, this study provides a novel investigation of the impact of natural fractures on the hydraulic fracturing process. Key geometrical features of the pre-existing fracture networks, including their orientation with respect to in-situ stress, position distribution, and heterogeneity of fracture cement strength, are considered. Furthermore, building on the insights from Zhu et al. (2023), the most influential factors—such as injection rate and fluid viscosity—are incorporated. The initiation, propagation, and formation of complex fracture networks are quantified using the newly proposed connectivity metric.

The arrangement of the paper is as follows: Section 2 introduces detailed information about the simulation scheme and also the novel connectivity metric for complex multi-cluster systems. Section 3 demonstrates impacts of natural fracture networks and operational factors on hydraulic fracturing process. Connectivity variations and flow behavior in the generated fracture network are also included in Section 3. In Section 4, the limitations of the method and possible improvements of the work are discussed. Section 5 summarizes important conclusions.

## 2. Materials and Methods

### 2.1. Simulation of Hydraulic Fracturing Process

The hydraulic fracturing process is a complex hydro-mechanical process, which requires separate methods to calculate solid deformation and fluid flow. In this work, we redeveloped an open-source multi-physics simulation

software, MECHSys, to conduct the hydraulic fracturing simulation (Galindo-Torres et al., 2012). For the solid deformation calculation, the software adopted the discrete element method (DEM), which does not require high mesh quality and complicated treatment for complex boundary conditions like other continuum methods. Rock masses are treated as an assembly of discrete particles, represented by polyhedrons. Linear contact and bonding models are implemented to approximate the interactions between particles (Galindo-Torres et al., 2012). More detailed information on the DEM-LBM method is provided in Text S1 in Supporting Information S1.

The criterion of fracture initiation is constrained by a threshold value on the total strain, denoted as  $\epsilon_{th}$ .

$$|\vec{\epsilon}_n| + |\vec{\epsilon}_t| \geq \epsilon_{th}, \quad (1)$$

where  $\vec{\epsilon}_n$  and  $\vec{\epsilon}_t$  are the normal and tangential strain caused by the displacement of adjacent faces. For intact rock grains, the threshold value is set as 0.01. The threshold value will determine the rock strength considering the constant elastic modulus and stiffness adopted in this work. A larger threshold value means that the rock can sustain higher levels of strain and larger stress are required before failure.

Natural fractures are simulated by modifying the strengths of bonds. Fractures are highly permeable at initiation, while their aperture will be reduced after a long geological history with compressive load and cement refilling (S. E. Laubach, 2003; Ukar & Laubach, 2016). In addition, the strength of natural fractures with sealing depends on the cement type (such as calcite or quartz) and shows heterogeneous characteristics. Since the spatial distribution of cement and sealing patterns is usually unknown, a Weibull distribution is adopted to generate various bond strengths and mimic the heterogeneous nature of fracture cements (Z. Chen & Wang, 2017; Van Mier et al., 2002).

$$f(\epsilon_{th}) = \frac{m}{\epsilon_{th}^0} \left( \frac{\epsilon_{th}}{\epsilon_{th}^0} \right)^{m-1} \exp\left(-\left(\frac{\epsilon_{th}}{\epsilon_{th}^0}\right)^m\right), \quad (2)$$

where  $\epsilon_{th}^0$  is the average bond strength threshold and is set as 0.005 (half of the intact rock strength) in this work.  $m$  is the shape parameter, describing the heterogeneity degree of the bond strength. An infinitely large  $m$  corresponds to a homogeneous strength distribution, while a low value of  $m$  indicates a heterogeneous distribution.

To incorporate natural fractures into the DEM scheme, the natural fractures are initially generated as discrete fracture networks by HatchFrac (Zhu, Khirevich, & Patzek, 2022). The fracture geometries are described by different statistical distributions. The fracture length follows a power-law distribution with an exponent of 2.2, as natural fracture networks typically exhibit exponents ranging between 2 and 3 (Zhu et al., 2018). The orientation of natural fractures follows a von Mises-Fisher distribution with a small concentration parameter,  $\kappa$ , indicating a close-to-uniform distribution of orientations, as observed in outcrop maps (Zhu, He, Santoso, et al., 2022). In this work, we set the concentration parameter  $\kappa$  to 3.7 but consider different mean orientations with respect to the maximum stress (left-right direction). Clustering effects, which are common in natural fracture networks, are described by a fractal spatial density distribution characterized by a fractal dimension,  $F_D$ . An over-percolative state is also considered, where the fracture intensity is much higher than the intensity required to form a spanning fracture cluster, a phenomenon frequently observed in natural fracture networks (Zhu, Lei, et al., 2022). One example of a generated DFN is shown in Figure 1c. Detailed information on generating discrete fracture networks with pre-defined statistical distributions for key fracture geometries is provided in Text S6 in Supporting Information S1.

After generating the discrete fracture networks, we check the intersection between the DFN and all particle bonds. If a bond intersects with a natural fracture, it becomes a natural fracture segment, and its strength follows the Weibull strength distribution (Equation 2). By doing so, we embed the natural fracture networks inside the DEM scheme as shown in Figure 1b. Therefore, pre-existing natural fractures are represented by particle bonds. To capture the geometrical details of these fractures, the number of particles should be large enough. In this work, the calculation domain is 20 cm  $\times$  20 cm with a thickness of  $1.28 \times 10^{-3}$  m, as shown in Figure 1. The system size is intentionally chosen to be large enough to ensure that a sufficient number of particles can be generated and that fracture propagation does not reach the boundary. The total number of particles is 12,421 with a uniform size distribution. During the Delaunay triangulation algorithm used for meshing, we provided a maximum particle area of  $5.0 \times 10^{-6}$  m<sup>2</sup> as input to ensure a high bond count and small bond sizes, accurately capturing natural fracture geometries. Four rectangular plates on each side of the domain are added to apply different stresses in the

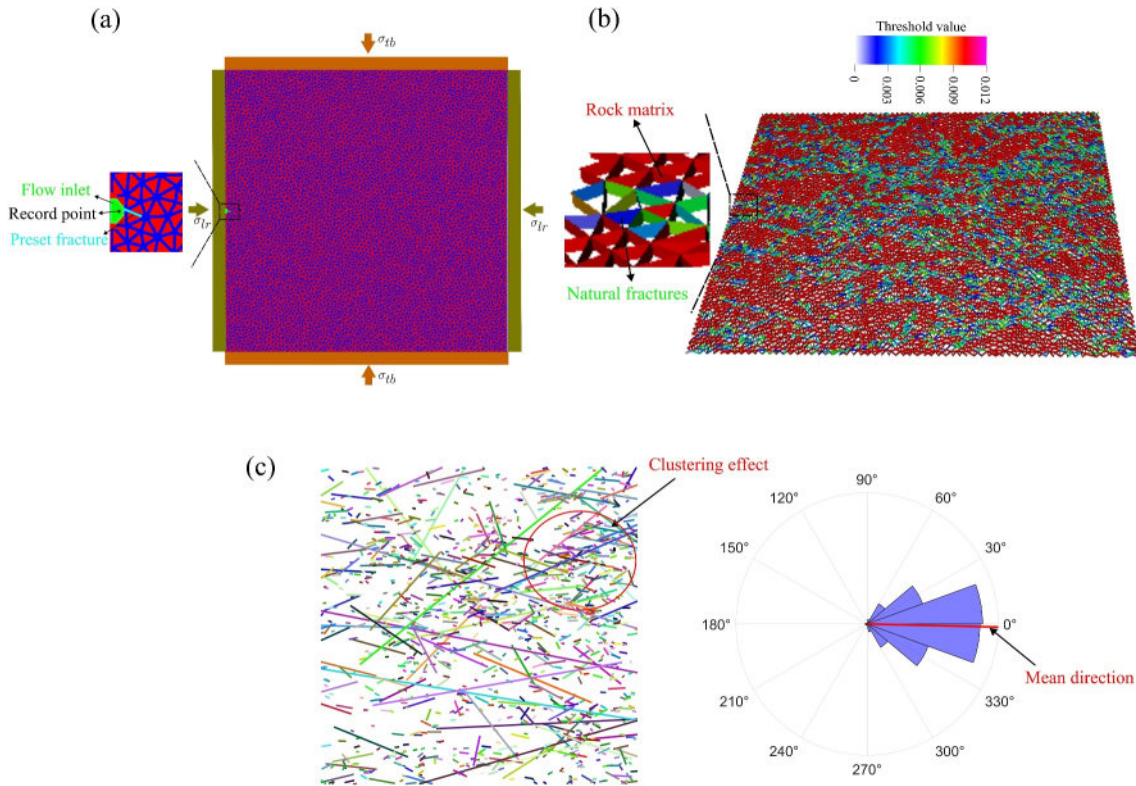


**Figure 1.** (a) The calculation domain has a length of 0.2 m, a width of 0.2 m, and a thickness of 1.28 mm. A fixed stress ratio,  $\sigma_{lr}/\sigma_{tb} = 1.5$ , and a constant solid volume fraction,  $\gamma = 0.97$ , are chosen. The fluid is injected from the flow inlet at a constant injection rate, and a fixed pressure is applied on the right side of the domain. A preset fracture is set to mimic the perforation process in reality. All other boundaries are set as solid. (b) Implementation of natural fractures in the discrete element method scheme (Case 1), where natural fractures are represented by different bonds with strengths following a Weibull distribution. Case 1 has  $m = 2$ , indicating strong heterogeneity in fracture strength. (c) The generated discrete fracture network of Case 1, where the fracture lengths follow a power-law distribution with an exponent of 2.2. The orientation follows a von Mises-Fisher distribution with a mean direction of  $0^\circ$  relative to the maximum stress (left-right direction) and a concentration degree of  $\kappa = 3.7$ . The position follows a fractal spatial density distribution with  $F_D = 1.7$ , exhibiting clustering effects. The rose diagram shows the orientation distribution with the mean direction denoted.

horizontal (left-right,  $\sigma_{lr}$ ) and vertical (top-bottom,  $\sigma_{tb}$ ) directions, as shown in Figure 1a. The horizontal and vertical plates are each 20 cm long, with a width and height equal to the particle thickness,  $1.28 \times 10^{-3}$  m. A constant flow rate is applied at the inlet, and a fixed pressure is assigned on the right side of the domain. All other boundaries are set as solid.

**Table 1**  
Input Parameters for the DEM-LBM Simulation

Parameter	Value
Normal contact stiffness, $K_n$	$1.0 \times 10^6$ N/m
Tangential contact stiffness, $K_t$	$1.0 \times 10^6$ N/m
Normal elastic modulus, $B_n$	$2.0 \times 10^6$ [Pa]
Tangential elastic modulus, $B_t$	$4.2 \times 10^6$ [Pa]
Matrix bond strength, $e_{th}$	0.01 [–]
Fluid density, $\rho_f^*$	$1.0 \times 10^3$ [kg/m <sup>3</sup> ]
Lattice size in LBM, $\delta_x^*$	$1.0 \times 10^{-4}$ [m]
Time step in DEM/LBM, $\delta_t^*$	$1.0 \times 10^{-6}$ [s]
Solid volume fraction, $\gamma$	0.97 [–]
Stress anisotropy, ( $\sigma_{lr}/\sigma_{tb}$ )	1.5 [–]

Detailed input parameters are summarized in Table 1. The stiffness and modulus are intentionally scaled to increase the time step in the DEM method; however, the other parameters are also correspondingly scaled based on a detailed Buckingham analysis in Zhu et al. (2023) and also available in Text S5 in Supporting Information S1. For example, a stress magnitude of 10 MPa in the experiment corresponds to  $1.68 \times 10^4$  Pa in the simulation. In this work, the stress anisotropy and solid volume fraction,  $\gamma$ , are also kept constant. The stress ratio between the horizontal and vertical stresses,  $\sigma_{lr}/\sigma_{tb}$ , is set to 1.5.  $\gamma$  is set to 0.97.  $\gamma$  is related to the permeability of the rock. The larger the  $\gamma$  value, the lower the permeability will be. In Zhu et al. (2023), the impacts of individual stress anisotropy or rock permeability on fracture network complexity are systematically investigated, with different stress ratios and  $\gamma$  values tested. Stress anisotropy influences the initiation pressure, where a larger stress value requires a larger initiation pressure. In terms of fracture geometries, it determines the fracture orientation (perpendicular to the minimum stress) but does not affect the complexity in a homogeneous rock mass.

$\gamma$  values also influence the initiation pressure, with a larger  $\gamma$ , indicating lower-permeability rocks, requiring a larger initiation pressure. However,  $\gamma$  does not significantly change the fracture geometry but affects the pressure propagation in the neighboring region. In this work, we intend to investigate the hydraulic fracturing process, which is usually implemented for low-permeable reservoirs; therefore, a large  $\gamma$  value is chosen.

For the fluid flow simulation, MECHSYS adopted the lattice Boltzmann method (LBM), which offers several advantages, including simple calculation procedures, convenient implementation of parallel computation, and straightforward treatment of complex geometries. Additionally, the LBM method can solve the Navier-Stokes equations through the Chapman-Enskog theory, which overcomes possible inaccuracies caused by the lubrication flow assumption. In this work, considering accuracy and computational efficiency, a D3Q15 model is adopted in the LBM scheme, and the corresponding evolution equation is:

$$f_i(\vec{x} + \vec{e}_i \delta t, t + \delta t) = f_i(\vec{x}, t) - \frac{\delta t}{\tau} (f_i(\vec{x}, t) - f_i^{eq}(\vec{x}, t)), \quad i = 0, 1, 2, \dots, 14, \quad (3)$$

where  $f_i$  and  $f_i^{eq}$  are the density distribution function and the corresponding equilibrium distribution in the  $i$ th discrete velocity direction,  $\vec{e}_i$ ,  $\delta t$  is the time step adopted in the simulation, and  $\tau$  is the relaxation time. The lattice size of the LBM is important, as it directly determines the computational complexity of the whole scheme. However, the lattice size should be small enough to capture the generated fractures and keep the scheme stable, with the relaxation time  $\tau$  in LBM larger than 0.5. In this work, the relaxation time is set to 0.53 with the chosen lattice size and time step, ensuring the stability of the method.

An immersed boundary method is applied to incorporate the fluid-solid interactions (Z. Chen & Wang, 2017; Noble & Torczynski, 1998). Detailed information on the DEM-LBM coupling method and its validation are summarized in Text S2–S4 in Supporting Information S1 and are also available in previous works (Z. Chen & Wang, 2017; Z. Chen, Elsworth, & Wang, 2020; Z. Chen & Wang, 2020; Zhu et al., 2023).

## 2.2. Connectivity Metric and Influential Factors

In this study, we adopt a straightforward yet powerful metric,  $C_i$ , for assessing the connectivity of natural fracture networks made up of multiple clusters (Zhu et al., 2024).

$$C_i = \sum_{i=0}^n \underbrace{\left( \frac{k_m \mu_w}{k_f \mu} \right) \left( 1 - \frac{d_i}{d_{\max}} \right)}_{\text{Interaction term}} \times \underbrace{\left( \frac{l_i}{l_{\text{total}}} \right)}_{\text{Individual term}} C_i \quad (4)$$

Here  $n$  is the number of fracture clusters;  $k_m$  and  $k_f$  are the matrix and fracture permeabilities, respectively;  $\mu$  and  $\mu_w$  are the viscosities of formation fluid at reservoir conditions and water at standard conditions, respectively;  $d_i$  represents the shortest distance in the matrix from cluster  $i$  to the central cluster;  $d_{\max}$  is the diagonal length of the bounding box that encloses all fractures in the considered fracture system;  $l_i$  denotes the total length of fractures in cluster  $i$ ;  $l_{\text{total}}$  is the total length of all fractures in the system; and  $C_i$  is the connectivity metric of cluster  $i$ . The parameters  $k_f$ ,  $\mu_w$ , and  $d_{\max}$  normalize the respective variables.

In this work, we focus more on the dynamic evolution of fracture networks and their connectivity, rather than the specific seepage process inside the fracture networks. Therefore, the coefficients related to permeability and fluid viscosity are standardized to 1 for the connectivity calculation. The primary hydraulic fracture is selected as the central cluster, referring to the fracture cluster initiated at the perforation site. To determine the shortest distance through the matrix using intermediate clusters, the fracture system is transformed into a connected graph, where each cluster is regarded as a node, and the shortest distance between clusters is assigned as the distance between nodes. The Dijkstra algorithm (Cormen et al., 2022) is applied to find the shortest paths between any arbitrary cluster and the central cluster. For an individual term,  $C_i$  can represent any connectivity metric for cluster  $i$ . In this study, we adopt the average number of links per branch as the connectivity metric (Sanderson & Nixon, 2015), which is sufficient since variable fracture apertures are excluded from the subsequent analysis of the fracture networks.

**Table 2**  
*Influential Factors in the Hydraulic Fracturing Process*

Factor	Low	Intermediate	High	Definition
$\mu$ & $\kappa$	$\mu = 0, \kappa = 3.7$	$\mu = \pi/6, \kappa = 3.7$	$\mu = \pi/3, \kappa = 3.7$	$\mu$ is the mean orientation with respect to the maximum stress and $\kappa$ is the concentration degree
$F_D$	1.7	1.9	2.0	The fractal dimension in a fractal spatial density distribution
$m$	2	5	10	Heterogeneity degree of the fracture strength
$u$	0.2	0.3	0.5	Injection rate, unit [m/s]
$\nu$	1	5	–	Fluid viscosity, unit [ $10^{-4}$ m <sup>2</sup> /s]

$$C_i = \frac{3 \times N_T + 4 \times N_X}{N_B}, \quad (5)$$

where  $N_T$ ,  $N_X$ , and  $N_B$  refer to the numbers of  $T$ -type,  $X$ -type nodes and branches.  $N_B$  is calculated with  $1/2(N_I + 3N_T + 4N_X)$  and  $N_I$  is the number of  $I$ -type nodes.

As a result,  $C_i$  is a dimensionless number between 0 and 2.0, with a larger value indicating better connectivity. Detailed information on the calculation of  $C_i$  is summarized in Text S7 in Supporting Information S1. More detailed information on total connectivity and the influential factors, including fracture sealing, central cluster selection, and cluster linkages, is systematically investigated in the previous research work (Zhu et al., 2024).

The hydraulic fracturing process is complex and influenced by many factors, such as in-situ stress anisotropy, injection rate, fluid viscosity, rock permeability, and rock strength heterogeneity. It is extremely expensive to traverse all influential factors with the DEM-LBM scheme. The impact of individual factors on the hydraulic fracturing process is systematically investigated in Zhu et al. (2023), where injection rate and heterogeneity of the rock mass are identified as the most important influential factors on the complexity of generated fracture networks. The other factors do have an impact on the initiation of fractures, but they do not significantly change the final fracture geometries. Among these factors, the injection rate and fluid viscosity are operational parameters that can be adjusted artificially. Hence, this study considers various fluid viscosities and injection rates. The remaining factors represent intrinsic formation or rock characteristics, which vary depending on the specific engineering site, and typical constant values are assigned to these factors. The in-situ stress has a fixed ratio of 1.5. Rock permeability is characterized by the solid volume fraction and set to 0.97, indicating low permeability for the rock matrix. Rock strength heterogeneity is not separately considered since we account for the strength heterogeneity of natural fractures.

In total, we consider five influential factors in the hydraulic fracturing process: three factors related to preexisting natural fractures, including the mean orientation toward the maximum stress ( $\mu$ ), the fractal dimension for the clustering effect ( $F_D$ ), and the heterogeneity degree ( $m$ ) for the fracture strengths; and two factors related to the operational scheme, injection rate, and fluid viscosity. In practice, slickwater is usually chosen as the fracturing fluid (Barati & Liang, 2014); therefore, we use two levels of fluid viscosity at low values for consideration. The other four factors are considered at three levels. To ensure computational affordability, we conduct a Taguchi Design with 18 cases. The considered parameters are summarized in Table 2, and the detailed design results are shown in Table 3.

### 3. Results

#### 3.1. Fracture Initiation and Propagation Behavior

The pore pressure at the recording point for 18 cases is shown in Figure 2. Different conditions lead to different initiation pressures, and we have summarized the cases into three categories considering low, intermediate, and high initiation pressures, indicated by different colors for better illustration. Cases with low initiation pressures include cases 1, 2, 5, 6, 7, 8, and 9; intermediate pressures include cases 3, 10, 11, 14, 17, and 18; high pressures include cases 4, 12, 13, 15, and 16. Comparing different input parameters for cases in Table 3, it shows that injection rate and viscosity are important and control the initiation pressure. A correlation analysis between these factors and initiation pressure yields correlation coefficients of 0.44 and 0.51. Therefore, they are positively

**Table 3**  
Taguchi Design for Five Factors in the Hydraulic Fracturing Process

No.	$\mu$	$F_D$	m	u	$\nu$
1	0	1.7	2	0.2	1
2	0	1.9	5	0.3	1
3	0	2.0	10	0.5	1
4	$\pi/6$	1.7	5	0.5	1
5	$\pi/6$	1.9	10	0.2	1
6	$\pi/6$	2.0	2	0.3	1
7	$\pi/3$	1.7	10	0.3	1
8	$\pi/3$	1.9	2	0.5	1
9	$\pi/3$	2.0	5	0.2	1
10	0	1.7	2	0.2	5
11	0	1.9	5	0.3	5
12	0	2.0	10	0.5	5
13	$\pi/6$	1.7	5	0.5	5
14	$\pi/6$	1.9	10	0.2	5
15	$\pi/6$	2.0	2	0.3	5
16	$\pi/3$	1.7	10	0.3	5
17	$\pi/3$	1.9	2	0.5	5
18	$\pi/3$	2.0	5	0.2	5

Note. The definition of each factor is shown in Table 2.

correlated with the initial pressure; a higher injection rate and larger fluid viscosity lead to a higher initiation pressure, which aligns with the conclusions of prior researches (Duan et al., 2018; Morgan et al., 2017; Zhu et al., 2023). Heterogeneity of rock strength should also impact the initiation pressure. However, the correlation is 0.06 for 18 cases, indicating that strength heterogeneity is almost irrelevant unless natural fractures intersect bonds at the inlet.

The variations in injection pressure can be attributed to several factors, with three key ones highlighted here. The first factor is the interplay between the injected fluid volume, the newly generated fracture volumes, and fluid leakage into the formation. When the injection rate exceeds and the newly generated fracture volumes and leakage volume, the injection pressure tends to rise, as seen in Cases 4 and 13, where high injection rates result in significant pressure increases after fracture initiation. The second factor involves the presence of strong bonds encountered during fracture propagation. Higher pressures are required to break stronger bonds, or overcome larger in-situ stresses to alter propagation direction. This phenomenon is frequently observed in laboratory experiments (Bahorich et al., 2012; Dehghan, 2020) and leads to irregular variations in injection pressure for all cases in this study due to non-homogeneous bond strength. In Case 15, which has a high degree of heterogeneity and moderate injection rate, a notable pressure increase occurs after 0.02 s. As shown in Figure 3, fracture propagation in Case 15, occurring from 0.0285 to 0.0435 s, does not exhibit significant changes, as the primary fracture cluster experiences limited growth. The third factor is the development of complex fracture networks, particularly the linkage between different clusters, which can cause a sharp reduction in injection pressure. For

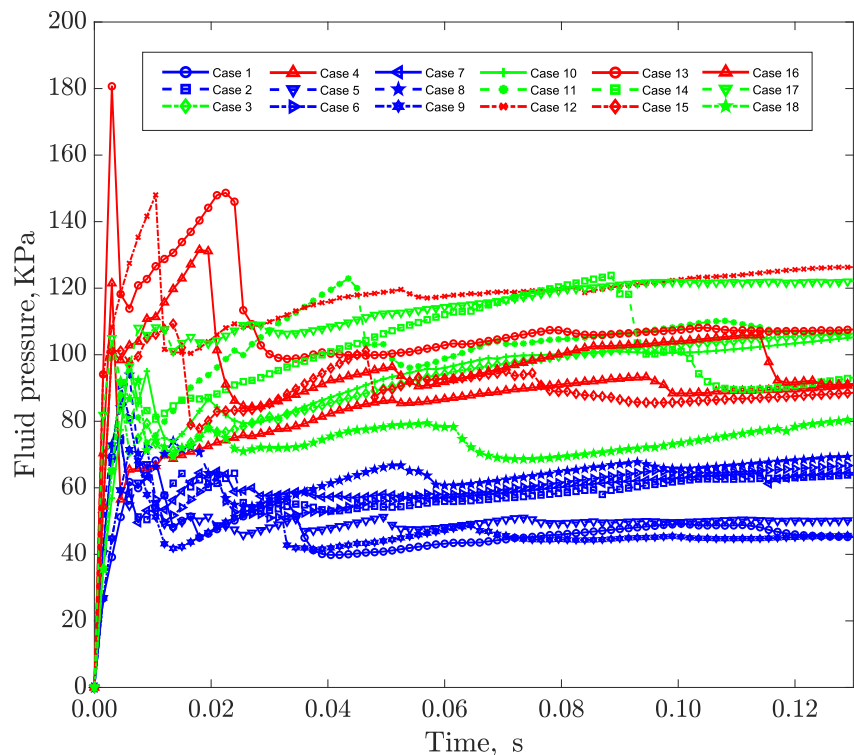


**Figure 2.** The pore pressure evolution at the recording point for 18 cases. The red, green, and blue colors represent three categories based on initiation pressure: low, intermediate, and high initiation pressures.

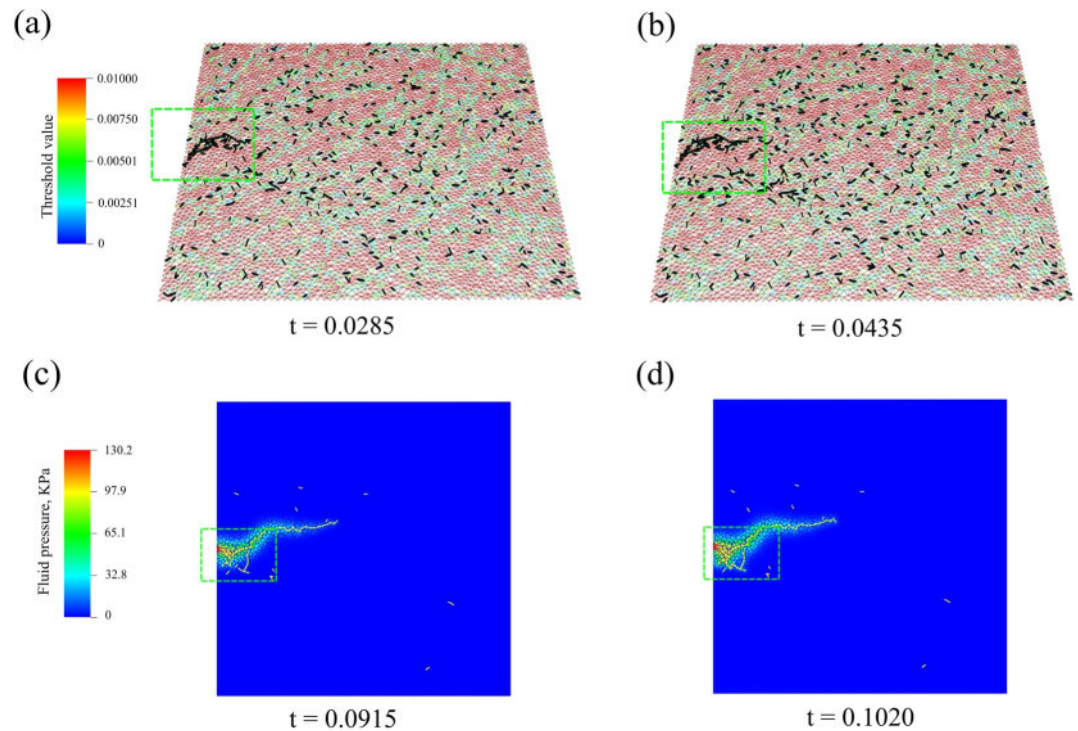


**Figure 3.** Upper panel: In Case 15, fracture propagation occurs between 0.0285 s (a) and 0.0435 s (b). Minimal changes are observed, as the primary fracture cluster shows limited growth due to strong surrounding bonds, which would require higher injection pressures to break. Lower panel: In Case 14, fracture propagation from 0.0915 s (c) to 0.1020 s (d) shows local clusters connecting with the primary fracture cluster, leading to a decrease in injection pressure. The background illustrates the fluid pressure distribution.

instance, in Case 14, after 0.091 s, the injection pressure decreases sharply when the primary fracture cluster connects with a local cluster. The fracture propagation in Case 14, shown from 0.0915 to 0.1020 s in Figures 3c and 3d, illustrates the impact of cluster linkage. In general, these pressure variations result from a combination of multiple factors, with each factor potentially dominating the process under specific conditions.

The fracture propagation in Case 1 and Case 3 are shown in Figures 4 and 6 as examples. Case 1 has severe heterogeneity in the natural fracture strength and a low injection rate, while Case 3 has much more homogeneous fracture strength and a high injection rate. The fracture networks generated in these two cases are significantly different and representative for analysis. Both cases have natural fractures distributed in the neighborhood of the inlet. The primary hydraulic fracture initiated in the natural fracture bonds and tends to propagate in the direction perpendicular to the minimum principal stress (left to right). Both tensile and shear fractures are generated in the hydraulic fracturing process. The actual stress states of rock masses can be complex, involving a mix of stress components, so fractures can also have mixed shear and tensile strain components. In this work, a shear fracture is defined as the broken bond with a larger shear strain than the tensile strain. Similarly, a tensile fracture occurs when the tensile strain surpasses the shear strain in the broken bond. Similar classification is adopted by many researchers (Z. Chen & Wang, 2017; Shimizu et al., 2011).

The tensile fractures mainly exist in the primary hydraulic fracture as shown in Figures 4d and 6c. Shear fractures usually dominate in the final fracture networks, and they occur not only in the primary hydraulic fracture but also mostly in the isolated local clusters as shown in Figures 4d, 6c, and 6d. Those isolated local clusters are disconnected from the primary hydraulic fracture and form a multi-cluster fracture network. The proportion of the shear fractures in the final fracture networks is summarized in Table 4. In heterogeneous cases, most fractures generated are shear fractures instead of tensile fractures, especially for the local fracture clusters. Those local clusters are mainly due to pre-existing fractures with low strength and altered in-situ stress therein, which have also been observed by many other researchers (Taleghani & Olson, 2014; Wang et al., 2024; Zhu et al., 2023). Most cases have shear fractures more than 70%, except for cases 5 and 14, where only 55% and 64% of fractures

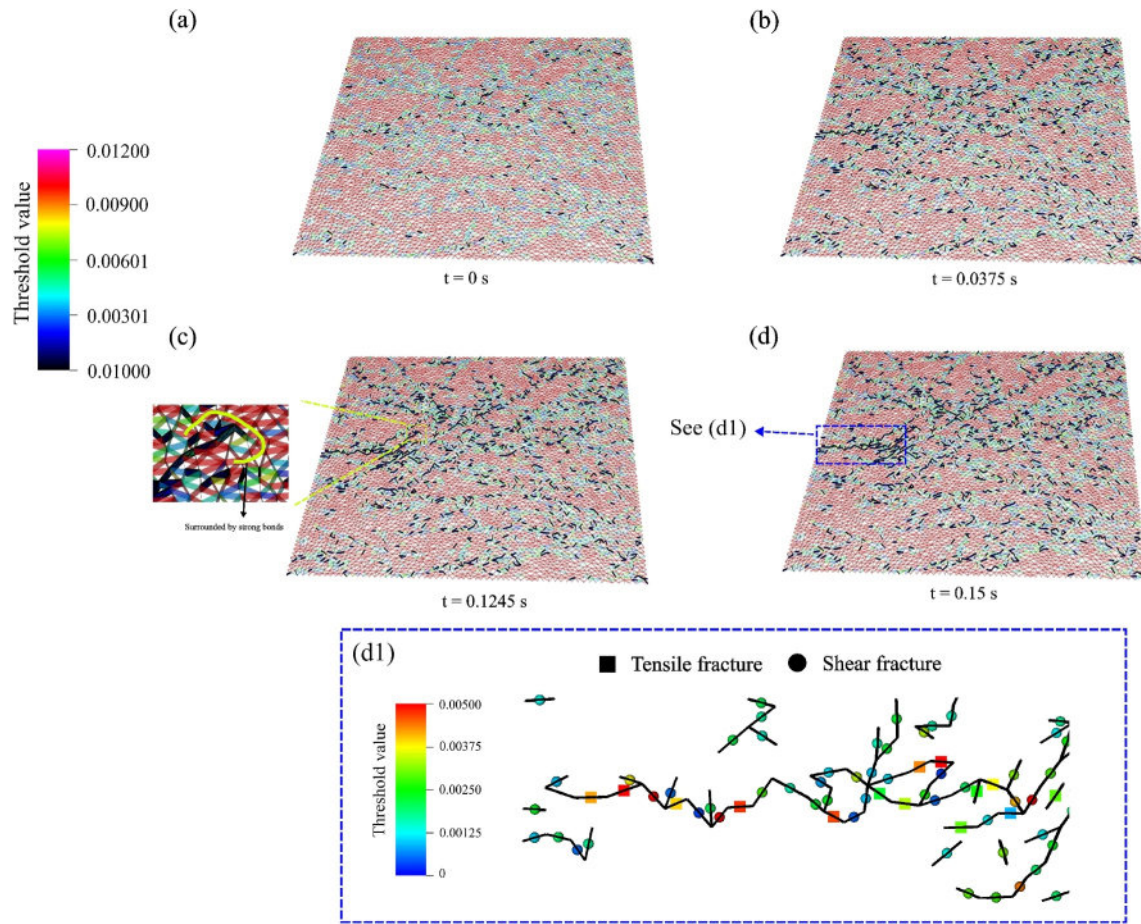


**Figure 4.** Fracture propagation at different times in Case 1. When strong bonds are encountered along the fracture propagation path, as shown in the zoomed figure in (c), higher injection pressure is required to break the bonds and continue propagation. The fracture types in the zoomed region are shown in (d1), where each fracture segment is marked with squares for tensile fractures and circles for shear fractures, while the color gradient from red to blue indicates decreasing fracture strength. Tensile fractures are mainly generated in the primary hydraulic fracture cluster, which has higher strength, while many shear fractures occur in both the primary hydraulic fracture cluster and local clusters.

are shear fractures, respectively. Both Cases 5 and 14 have much homogeneous strength distribution and a small injection rate.

In Case 1, with strong heterogeneities ( $m = 2$ ), many extremely weak bonds exist in the system. These bonds break at simulation onset due to imposed in-situ stress, irrespective of injected pressure, as shown in Figure 4a. In reality, sealed natural fractures can be reactivated under the current in-situ stress and provide hydraulic responses, as observed in C. A. Barton et al. (1995)'s work. Besides reactivated natural fractures, the sealing patterns of natural fractures can be complex, such as thin rinds, veneers, or bridge structures depending on the chemistry of reservoir fluids, fluid pressure, and temperature (S. Laubach et al., 2004). Therefore, natural fracture networks can be partially sealed with open segments. Those initially open fractures can also serve as nuclei for natural fracture growth.

With increasing pore pressure in the primary hydraulic fracture and pressure propagation to neighboring regions, the local stresses close to the primary hydraulic fractures are altered. Figures 5 and 7 show the shear force distribution for Case 1 and 3 at different time steps. It is obvious that the shear force in the neighboring regions around the primary hydraulic fractures increases, which causes sealed natural fractures to be reactivated, especially those with low strength as shown in Figures 4b–4d. There are some boundary effects at corners introduced by the implementation of remote stresses. The shear force at the corner does not change much if the stress disturbance from the primary hydraulic fracture is not significant, as shown in Figure 5. The magnitude and orientation do not change much during the hydraulic fracturing process. However, if the influence from the

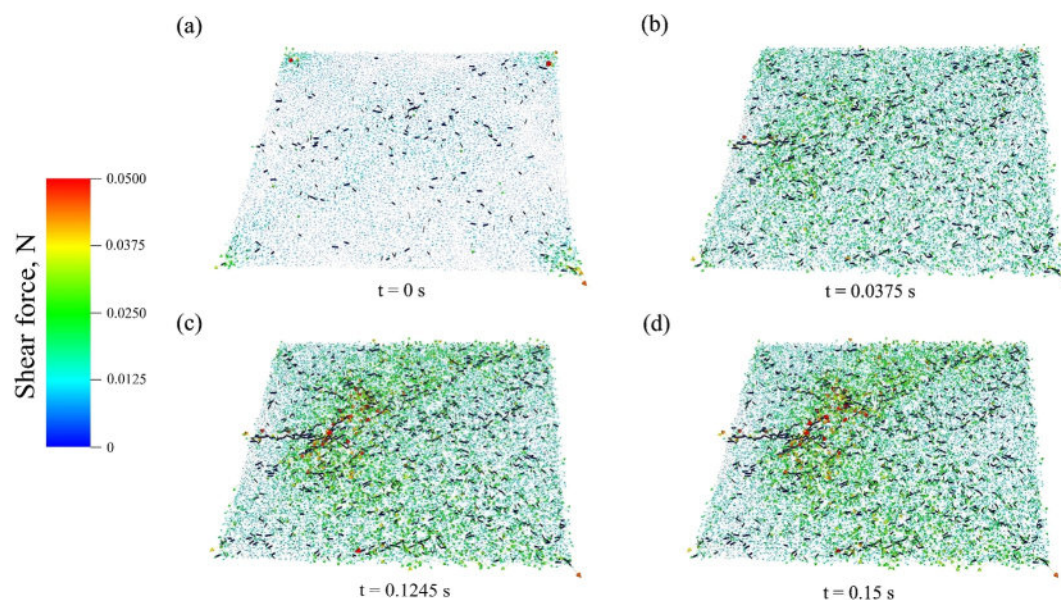


**Figure 5.** Shear force evolution at different times in Case 1 with severe heterogeneity in strength, in units of N. Numerous extremely weak bonds are present in the system at time zero (a). The shear force in regions surrounding the primary hydraulic fractures increases, as shown in (b)–(d).

primary hydraulic fracture has reached the corner region, there will be a superposition effect on the stress, as shown in Figures 7c and 7d. The shear force at the right-bottom corner has significantly increased and caused many weak bonds close to the corner to reactivate and form relatively large local clusters. Although the boundary effect is artificially caused by the implementation of boundary plates, it can represent possible heterogeneous in-situ stress distribution in reality. For example, the stress distribution close to a large natural fault. The superposition of stress can be significant and reactivate the sealed fractures, especially for those fractures with weak cements.

The interaction between hydraulic fractures depends largely on fracture strength and approaching orientations (Z. Chen, Yang, & Wang, 2018). However, in this study, a fracture comprises many segments (particle bonds) with varying orientations, complicating the decoupling of fracture orientation and strength impacts. Observations of fracture propagation indicate a tendency to propagate along weak bonds, halted by strong bonds. In Figures 4c and 4d, the primary hydraulic fracture stops propagating after 0.1245 s because the front is surrounded by strong bonds. The injection rate of Case 1 is small, which cannot provide enough pore pressure to break the strong bonds as shown in Figure 2. The hydraulic fracturing process is almost stopped with a few weak bonds reactivated, and the shear force distribution remains almost unchanged as observed in Figures 5c and 5d. Even if the fracture front is surrounded by strong bonds, but the pore pressure is large enough, it is possible for the hydraulic fracture to penetrate the strong bonds and continue to propagate in the original direction, as observed in Figures 6b and 6c. As observed in Figure 2, the pore pressure at the recorded point in Case 3 continues to increase after 0.0375 s, and it becomes large enough to break strong bonds after accumulation.

The existence of natural fractures and their diverse strengths are pivotal for the propagation of primary hydraulic fractures and the reactivation of preexisting natural fractures, thus influencing the final generated fracture networks. Heterogeneous cases tend to form much more complex fracture networks with many local clusters, while homogeneous cases tend to have simpler fracture networks dominated by the primary hydraulic fracture.

### 3.2. Connectivity Evolution and Flow Behavior

The generated fracture network from the hydraulic fracturing process is typically a multi-cluster system. Many local clusters are generated due to the altered in-situ stress caused by the injected high-pressure fluid as observed in previous section. Therefore, the connectivity defined in Equation 4 is used to quantify the connectivity of fracture networks at different time steps. The total connectivity can be further decomposed into two parts. One is

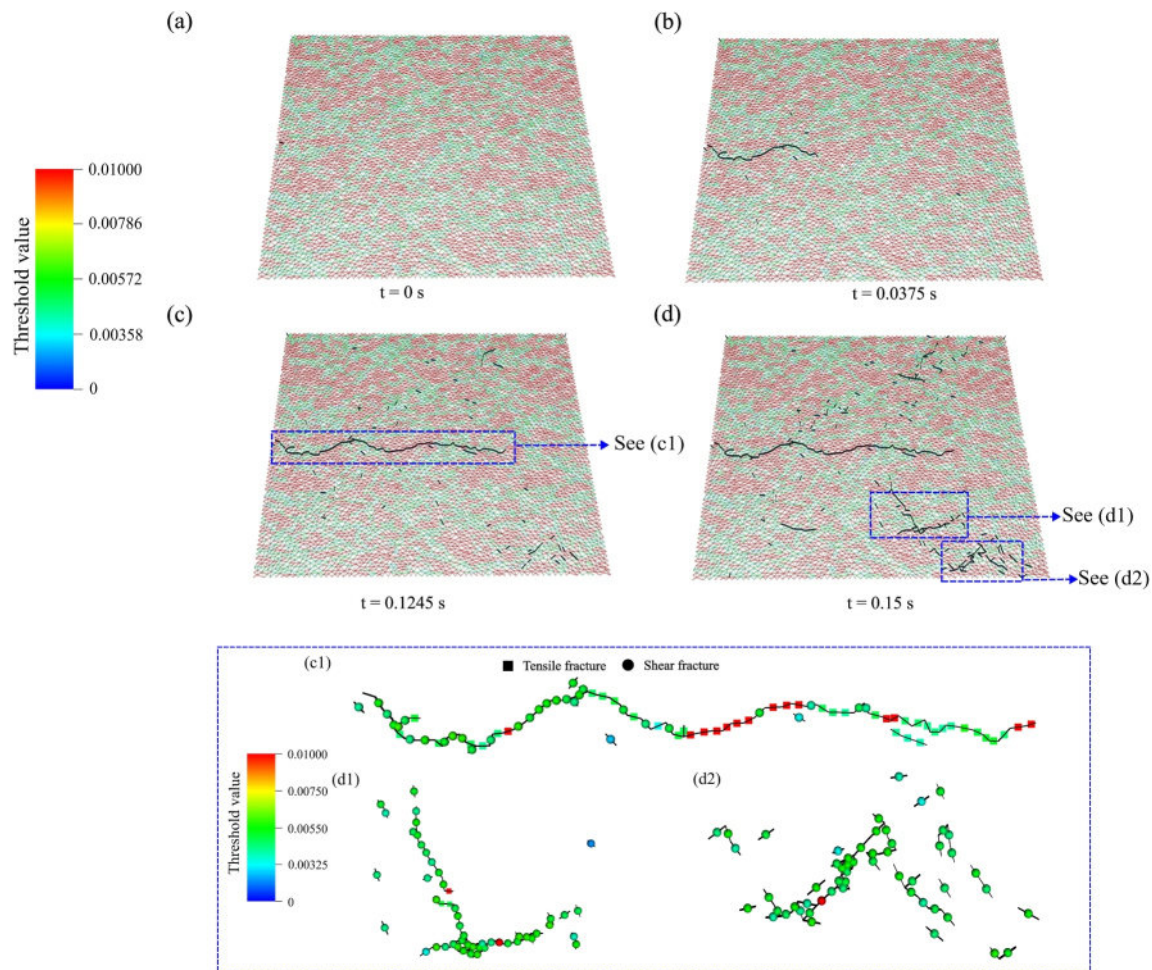


**Figure 6.** Fracture propagation at different times in Case 3 with weak heterogeneity in strength. The fracture propagates by enlarging the primary hydraulic fracture cluster, with few local fractures generated. Tensile fractures are mainly formed in the primary hydraulic fracture clusters, as shown in the zoomed figure (c1). When the influence from the primary hydraulic fracture reaches the corner region, it leads to a superposition effect on the stress, causing low-strength bonds to break in shear and forming local clusters, as shown in the zoomed figures (d1) and (d2).

the contribution from the largest cluster, and the second one is from the local clusters. In the hydraulic fracture process, the largest cluster is usually the cluster where the primary hydraulic fracture belongs.

In Figure 8, the total connectivity of the entire fracture network and the largest cluster are shown in subfigures (a) and (b), respectively. The total length of generated fracture networks and the largest cluster are shown in subfigures (c) and (d). In addition, we also show the contribution from the largest cluster to the total connectivity and length in subfigures (e) and (f). For all cases, the length of the total fracture networks and the largest cluster increases with increasing time as expected.

The total connectivity usually exhibits an increasing trend in most cases, attributed to the increase in connectivity from both the largest clusters and local clusters. In Table 4, we also show the maximum connectivity of each case during the hydraulic fracturing process, as well as the connectivity at  $t = 0.135$ , where we stop recording data. The maximum connectivity is 1.82 in Case 12, where the largest cluster contributed to 94.8% of the total connectivity. However, with fracture propagation and the formation of local clusters, the overall connectivity can also decrease, resulting in half of the cases having smaller connectivity at the end. For example, Cases 3, 12, and 18 show obvious decreases after the connectivity reaches its maximum value. In Figure 8b and Table 4, the connectivity of the largest cluster also experiences a non-monotonic increase during the process; 14 out of 18 cases have smaller connectivity at the end, including Case 3, 12 and 18. The formation of local clusters typically decreases the connectivity of the largest cluster because it reduces the length coefficient in the individual term

**Table 4**  
*Connectivity and Shear Proportions Summary*

Case	Shear proportion	$C_i(\text{Max})$ (entire)	$C_i(\text{End})$ (entire)	$C_i(\text{Max})$ (largest)	$C_i(\text{End})$ (largest)	Proportion (Max) (%)	Proportion (End) (%)
1	0.91	1.030	1.030	0.080	0.079	7.8	7.8
2	0.79	1.222	1.207	0.518	0.478	42.4	39.6
3	0.82	1.221	1.101	0.974	0.390	79.8	35.4
4	0.89	1.435	1.435	0.580	0.369	40.4	25.7
5	0.55	1.131	1.125	0.875	0.769	77.3	68.4
6	0.92	1.086	1.086	0.105	0.092	9.6	8.4
7	0.71	1.473	1.473	1.277	1.277	86.6	86.6
8	0.93	1.207	1.207	0.295	0.295	24.5	24.5
9	0.76	1.214	1.197	0.643	0.611	53.0	51.0
10	0.96	1.215	1.215	0.281	0.281	23.1	23.1
11	0.95	1.495	1.495	1.022	0.997	68.3	66.6
12	0.93	1.821	1.719	1.727	1.516	94.8	88.2
13	0.96	1.723	1.719	1.516	1.516	88.0	88.2
14	0.64	1.533	1.504	1.356	1.300	88.5	86.5
15	0.95	1.249	1.249	0.250	0.223	20.0	17.8
16	0.90	1.727	1.704	1.585	1.548	91.8	90.8
17	0.96	1.476	1.476	0.869	0.862	58.9	58.4
18	0.92	1.468	1.372	1.159	0.905	78.9	66.0

Note. "Entire" refers to the fracture network composed of all clusters; "Largest" refers to the largest cluster; " $C_i(\text{Max})$ " refers to the maximum connectivity value during the hydraulic fracturing process; " $C_i(\text{End})$ " refers to the connectivity at  $t = 0.135$  s; and "Proportion" refers to the ratio of the connectivity of the largest cluster to the entire fracture network.

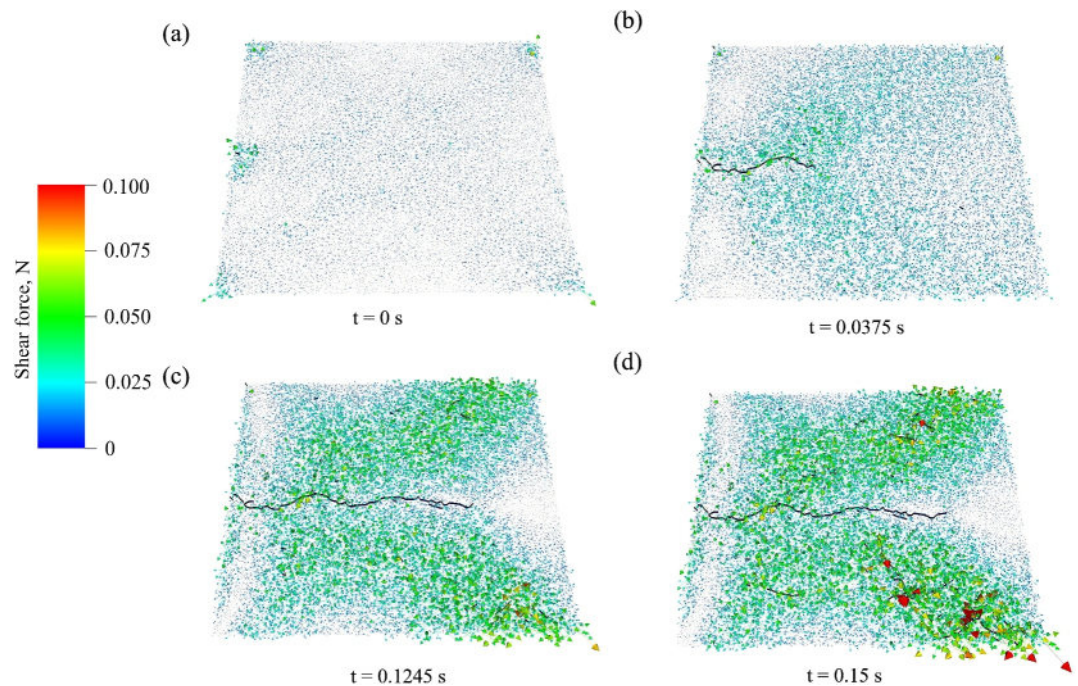


**Figure 7.** Shear force evolution at different times in Case 3 with weak heterogeneity in strength, in units of N. The shear force in regions surrounding the primary hydraulic fractures increases, as shown in (b)–(d). The influence from the primary hydraulic fracture has reached the corner region, leading to a superposition effect on the stress, as shown in (c) and (d).

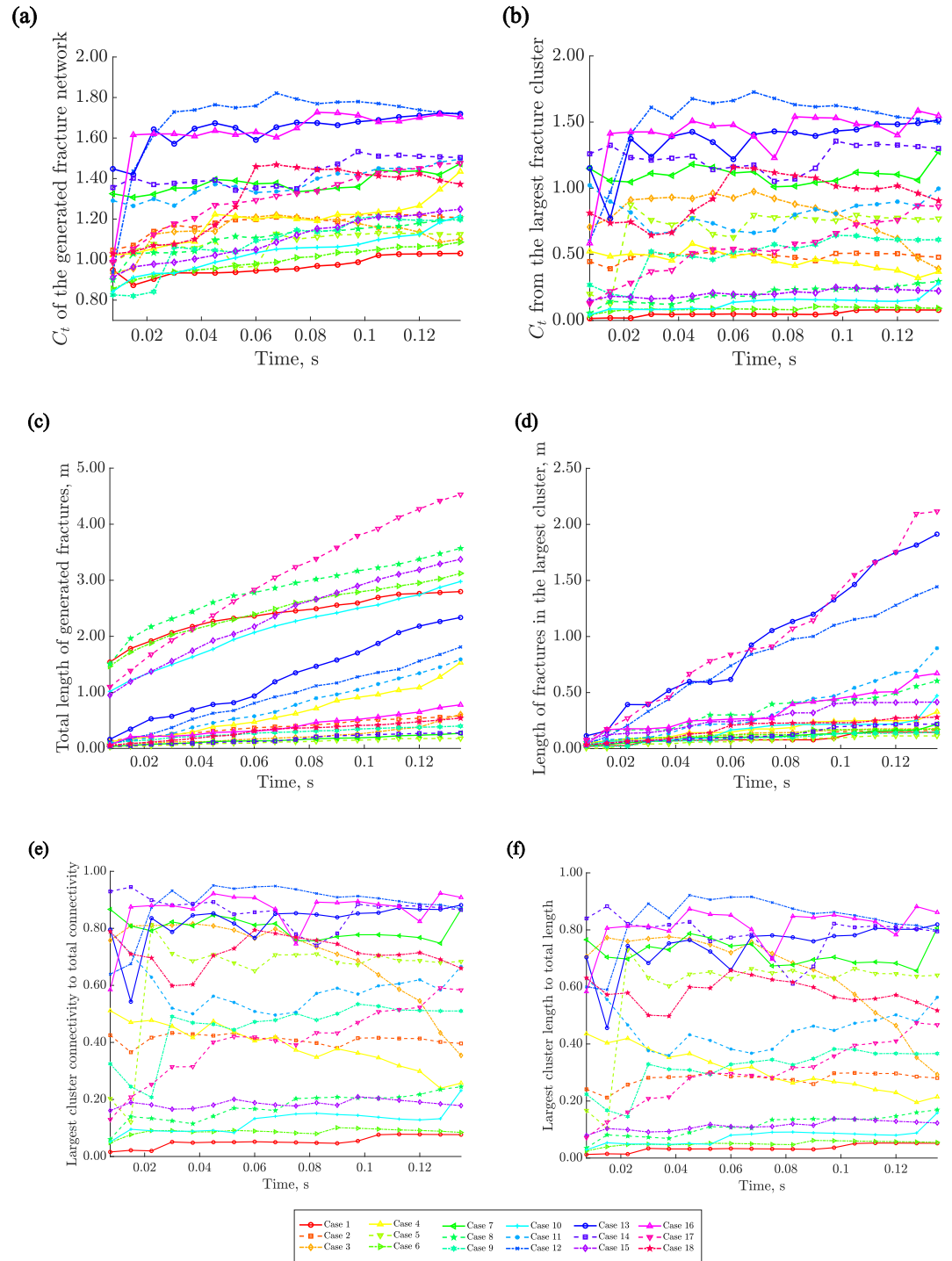


**Figure 8.** (a) Variations of total connectivity (b) Variations of connectivity contributed from the largest cluster (c) Variations of the total length of generated fractures (d) Variations of the total length of the fractures in the largest cluster (e) Proportion of connectivity contribution from the largest cluster (f) Proportion of total length contribution from the largest cluster.

$(l_{\text{largest}}/l_{\text{total}}) \cdot l_{\text{total}}$  increases with the formation of local clusters, while the increase in  $l_{\text{largest}}$  is insignificant. Additionally, all three cases have a relatively homogeneous strength distribution; therefore, the propagation of hydraulic fractures will not yield complex geometries with many T-type or X-type intersections. Consequently, the individual connectivity metric will not increase significantly. Although the formation of local clusters can

increase connectivity by boosting contributions from the local clusters, the increase from the local clusters cannot balance the decrease from the largest cluster, leading to an overall decrease in connectivity.

In Figure 8e, the proportions of connectivity contributed by the largest cluster and the total connectivity are demonstrated. The contribution from the largest cluster varies from case to case. Cases 1, 6, 8, 10, and 15 have a contribution from the largest cluster of less than 25%. The common characteristic for these cases is severe heterogeneity in fracture strengths. Therefore, in these heterogeneous cases, connectivity is mainly contributed by the local clusters, and the cluster formed by the primary hydraulic fractures only contributes a small proportion. The corresponding total length contribution is also similar, as shown in Figure 8f, where the fracture length in the largest cluster also contributes less than 20% of the total fracture length.

For cases 7, 13, 14 and 16, the contribution from the largest cluster to the total connectivity is almost larger than 80%. The common characteristic is that the heterogeneity degree is small in these cases. The final fracture networks are usually simple with fewer local clusters, and the primary hydraulic fractures compose the main part of the entire fracture networks. The largest cluster also contributes to the majority of fracture length, as shown in Figure 8f, where all these cases contribute to more than 80% of the fracture network. Comparing Figures 8e and 8f, similar variations are observed in the proportional contribution from the largest cluster to the total connectivity and total length, indicating a strong positive correlation between these two variables.

Case 12 exhibits the largest total connectivity, characterized by weak fracture strength variability, a large injection rate, and high viscosity. Conversely, Case 1 has the smallest total connectivity, featuring strong fracture strength variability, a small injection rate, and low viscosity. It's noteworthy that the case with the highest connectivity does not necessarily have the largest fracture length. For instance, Case 17 has the largest total length, while Case 5 has the minimum length. Case 5 is distinguished by a small injection rate, a more homogeneous distribution of fracture strengths, and low viscosity, whereas Case 17 has a large injection rate, high fluid viscosity, and severe fracture strength variability. The final fracture networks in Cases 12, 1, 17, and 5 are illustrated in Figure 9. Heterogeneity can contribute to generating complex fracture networks with multiple clusters, as depicted in Figure 9a, but it may not necessarily enhance overall connectivity. Fluid viscosity and injection rate play crucial roles in facilitating fluid pressure propagation to farther regions during the hydraulic fracturing process. In heterogeneous cases like Case 17, high fluid viscosity and a large injection rate facilitate the generation of more local clusters, whereas in homogeneous cases like Case 12, they help enlarge the cluster to which the primary cluster belongs.

To better illustrate the impact of the generated fracture network on fluid production in reality, a water-gas flow simulation is conducted to mimic the shale gas exploitation process. The final fracture networks in each case are embedded for the simulation, which is conducted in a reservoir simulation software, UNCONG (X. Li et al., 2015). A horizontal well is drilled at the left boundary. The permeability ratio between fracture and matrix is  $10^5$  to mimic a low-permeable reservoir. The simulation parameters are consistent with those chosen in Zhu, He, Li, et al. (2022).

The gas pressure distributions for Cases 1, 12, 5, and 17 are displayed in Figure 10. The simulation runs for 8 days before the pressure propagates to the boundary for better illustration. Following 8 days of production, the production ranking for the four cases is: Case 5 < Case 1 < Case 12 < Case 17. Analysis of the pressure distribution reveals that the pressure in the fractures connected to the production well can rapidly decrease due to the high permeability therein. However, isolated fracture clusters cannot contribute significantly to production due to the high resistance in the matrix. Similar results are observed in the study by Riffault et al. (2018), where they found that the microseismic cloud can be substantially larger than the associated stimulated fracture volume. These isolated fractures may be recorded as microseismic events but might not contribute to permeability enhancement or production increase for the production well. However, from a long-term perspective, local clusters can shorten the flow path in the low-permeable matrix, which can reduce the total resistance and contribute to production slowly.

To further demonstrate the relationship between connectivity and production, a correlation analysis was conducted. The correlation coefficient between connectivity and production is 0.60, indicating a positive correlation between these two variables, but obviously they are not equivalent. The correlation coefficient between total fracture length and production is 0.59, while the correlation coefficient between the length of the largest cluster and flow results is 0.77. This suggests that fluid production is primarily controlled by the largest cluster.

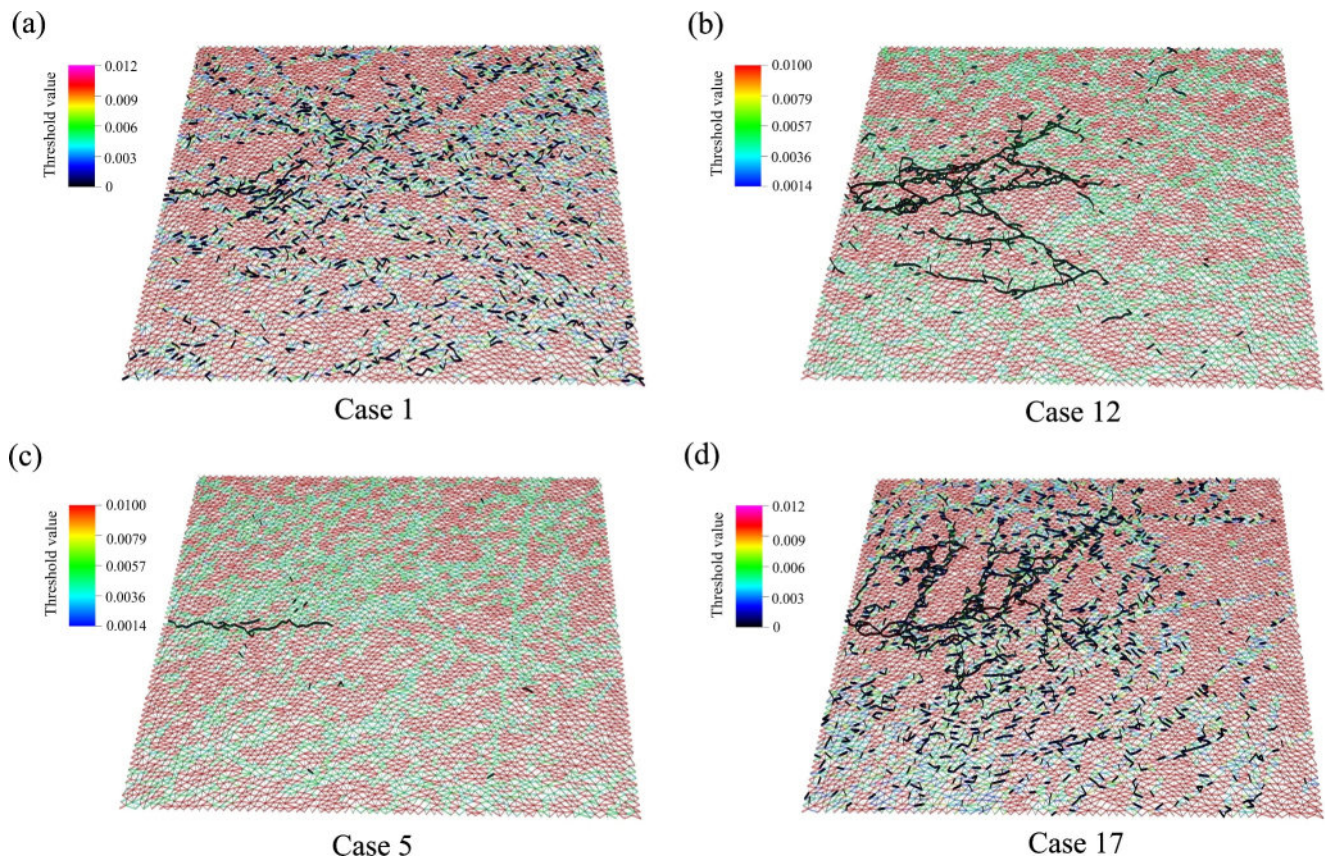


**Figure 9.** Final fracture networks generated in Cases 1, 12, 5, and 17, where Case 1 has the smallest connectivity, Case 12 has the largest connectivity, Case 5 has the shortest total fracture length, and Case 17 has the longest total fracture length.

Additionally, correlation coefficients between different factors and total connectivity  $C_t$  and fluid production are depicted in Figure 11. The results show that the mean orientation  $\mu$  has a positive correlation with the total connectivity and negligible correlation with fluid production. The correlation coefficients are 0.32 and 0.05, respectively. A larger mean orientation  $\mu$  indicates the natural fracture orientation is closer to the direction perpendicular to the maximum principal stress. The primary horizontal fractures tend to propagate perpendicular to the minimum principal stress. Therefore, the primary hydraulic fractures and the natural fractures tend to form an approximately orthogonal fracture network, like Case 17 in Figure 9d. Compared with fracture networks having a small orientation, like Case 12 in Figure 9b, orthogonal fracture networks tend to influence a much larger area and yield better total connectivity. However, it is also important to note that fractures oriented perpendicular to the maximum principal stress tend to remain in a mechanically stable state. They can break when the bond strength is significantly lower than the matrix. The fluid viscosity and injection rate have positive correlations with the total connectivity and production. The correlation coefficients between viscosity and connectivity, and between viscosity and production, are 0.64 and 0.65, respectively. For injection rate, the correlation coefficients are 0.29 and 0.61. Higher injection rate and viscosity can build up larger hydraulic pressure and cause more natural fracture breakage, forming much more complex fracture networks. Therefore, it is evident that they will have a positive correlation with connectivity and production.

The clustering effect parameter  $F_D$  has a negative correlation with both  $C_t$  and production (correlation coefficients of  $-0.38$  and  $-0.11$ ), respectively, indicating that the clustering effect can enhance the connectivity of the system and also contribute to the final production. The heterogeneity parameter  $m$  has a positive correlation with  $C_t$  (correlation coefficient of 0.33) but a negligible (slightly negative, with a correlation coefficient of  $-0.15$ ) correlation with production. As shown in Figure 8a, Case 12 has the largest total connectivity while it has weak heterogeneity, high injection rates and viscosity. Higher heterogeneity leads to a more diverse distribution of fracture strengths, with weak bonds easily reactivated during the hydraulic fracturing process, forming local

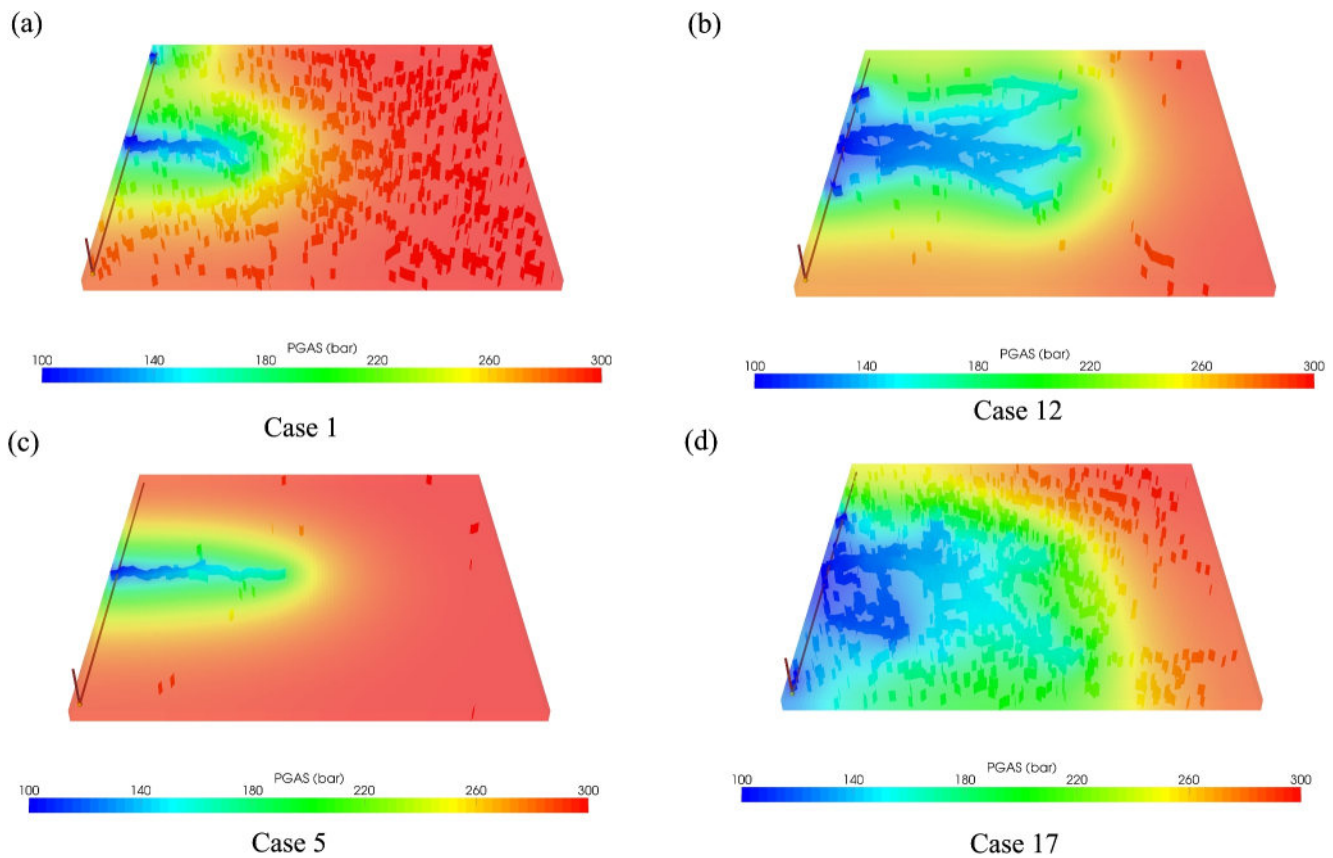


**Figure 10.** Pressure distribution in Case 1, 12, 5, 17 after 8 days of production. The water-gas flow simulation is conducted in a reservoir simulation software, UNCONG (X. Li et al., 2015). A horizontal well is drilled at the left boundary. The permeability ratio between fracture and matrix is  $10^5$  to mimic a low-permeable reservoir.

clusters. Although local clusters contribute to total connectivity, they also suppress the contribution from the largest cluster. In homogeneous cases, the fracture network is dominated by the largest cluster, and higher injection rates and viscosity tend to enlarge the largest cluster instead of forming more local clusters. Therefore, homogeneous fracture strength can help increase connectivity, especially when combined with high injection rates and viscosity. Regarding production, heterogeneous cases may cause many weak bonds to break, yielding a much larger total fracture length. If reactivated natural fractures directly or indirectly connect to the production well, they significantly contribute to production. However, if they remain disconnected from the production well, local clusters cannot contribute much to production due to high flow resistance in the matrix. Competition between these two mechanisms causes heterogeneity to have a negligible or even slightly negative impact on production.

#### 4. Discussion

In this work, we improved the DEM-LBM scheme to incorporate natural fractures, which better characterize the complex subsurface structures. Essential properties of the fracture networks, including fracture orientation, position distribution, and heterogeneous strength distribution, are considered. Additionally, operational parameters including injection rate and viscosity are taken into account. The dynamic evolution of subsurface structures under the coupled influences of factors is systematically investigated.

Natural fractures indeed bring much complexity and are essential for the propagation of hydraulic fractures. The heterogeneity of fracture strength determines the final fracture networks, with low-strength fractures breaking due to the altered in-situ stress and forming local clusters. Here, low-strength fractures refer to fractures with lower mechanical strength compared to the rock matrix and they have less resistance to shear or tensile failure. High injection rates and fluid viscosity result in a large pressure buildup and exaggerate the influential region. Besides the factors considered in this work, in-situ stresses and rock permeability are also important factors for hydraulic

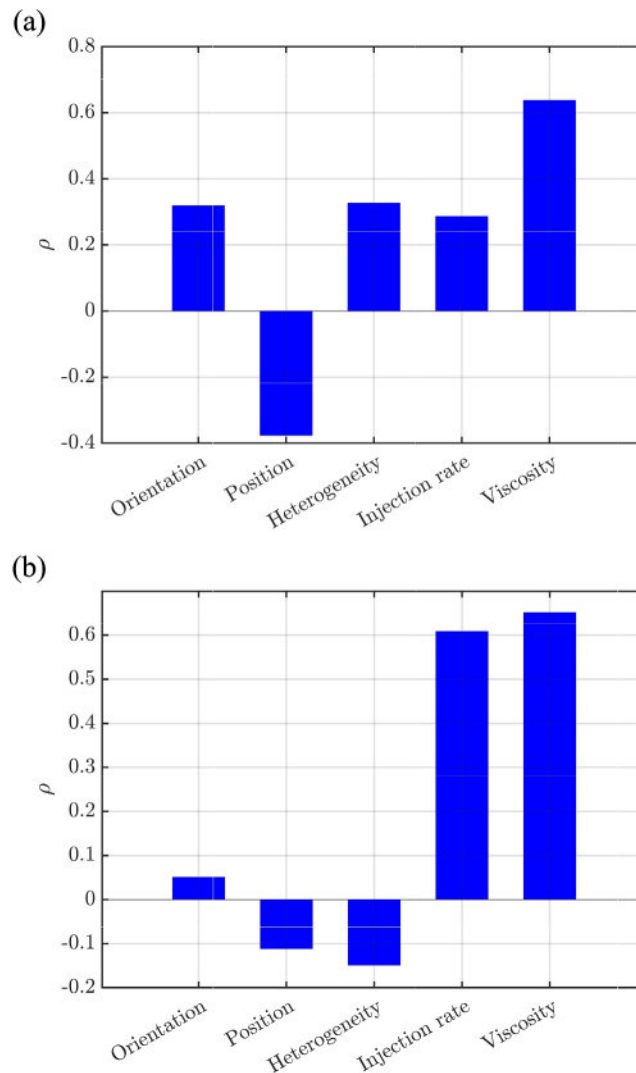


**Figure 11.** Correlation coefficients between different factors and the total connectivity  $C_t$  (a) and fluid production (b).

fracturing, but they are intrinsic formation parameters depending on the specific engineering field. A systematic investigation with various in-situ stresses and rock permeability is possible but computationally expensive.

Although the DEM-LBM scheme demonstrates strong adaptability in capturing key features during the hydraulic fracturing process, it has significant shortcomings, primarily due to its high computational intensity. The LBM method requires fine lattices to accurately capture the flow paths after the fracture generation, while the DEM method necessitates small time steps for convergence. In this work, the time step chosen is  $1.0 \times 10^{-6}$  seconds. Additionally, incorporating natural fracture networks demands a sufficiently large domain. Consequently, the computational time using the DEM-LBM scheme is substantial; we used 56 cores for parallel computing, and it required more than 15 days to run one case. Since actual rock masses are always three-dimensional, significant algorithmic optimization in terms of parallelization is necessary, along with considerably more computational resources.

In this work, we focus on particle interactions and local failure mechanisms, where DEM proves to be a suitable option. Additionally, we simulated brittle rock and its elastic behaviors. However, it is challenging to capture the elastic-plastic behavior of ductile rocks under certain loading conditions, such as high confining pressures where the material exhibits more ductile behavior. Therefore, for large-scale simulations or when ductile or plastic behavior dominates, other methods like FEM or continuum models may be more appropriate. In addition, to

simulate the hydraulic fracturing process in geothermal reservoirs, the thermal impact must be included, resulting in a hydro-thermal-mechanical coupling process (Z. Chen, Jin, & Wang, 2018; Z. Chen, Shu, et al., 2020), which could be the focus of future research.

The DEM-LBM coupled method is powerful for investigating the detailed fracture initiation and propagation process. However, all fracture formation and reactivation are represented by bond breakage between particles, and the breakage of particles is not possible in this scheme. However, particle breakage is usually observed in hydraulic fracturing with highly viscous fluid. In practical operations, low viscosity fluid is usually used for hydraulic fracturing due to its better injectivity. With the observations in this work, higher viscosity can also help to have greater pressure buildup and help to reactivate more natural fractures. Therefore, appropriate fluid viscosity is important for success in hydraulic fracturing operations.

The connectivity metric considered in this work is powerful for quantifying the connectivity of complex fracture networks composed of multiple clusters. In the calculation process shown in Equation 4, a central cluster should be selected to calculate the relative distance between clusters. However, if we calculate an average over all clusters, it eliminates dependence on the selection of the central cluster, ensuring a more robust and unbiased evaluation of network connectivity (Zhu et al., 2024). In this work, the central cluster is intentionally preserved, and the largest cluster where the primary fracture belongs is selected as the central cluster because the impact of the largest cluster is the main component of the final fracture networks and contributes much to the final production. The analysis in this work indicates that heterogeneous strengths can help increase total fracture length by activating more local clusters, while it may not help much with production due to the high resistance of the matrix. However, cases with many local clusters also have much potential to form larger and more connected fracture networks with continued injection of high-pressure fluid, but it may take longer operational time to achieve a successful fracturing outcome.

## 5. Conclusions

In this work, complex subsurface structures are characterized by discrete fracture networks, and their dynamic evolution, including fracture initiation, propagation, and connectivity variations during the hydraulic fracturing process, is systematically investigated. In particular, the impact of fracture orientations, position distributions, and strength variability, as well as injection rate and fluid viscosity, are considered. Several key conclusions are summarized below:

- Interactions between hydraulic fractures and natural fractures are important for hydraulic fracture propagation and final fracture networks. Fracture strength is a key factor for the interaction, and hydraulic fractures tend to propagate along natural fractures with low strength.
- Fracture strength variability can significantly impact the final fracture networks. Fractures with low strength will break due to altered in-situ stress and form local clusters. High injection rates and fluid viscosity result in a large pressure buildup, exaggerating the influential region and causing more low-strength fractures to break, mainly in shear failure mode. In cases with heterogeneous strength, shear fractures can account for more than 70%.
- A multi-cluster system is usually formed during the hydraulic fracturing process, and its connectivity can be well quantified using the proposed connectivity metric,  $C_l$ . This metric accounts for contributions from both the largest cluster and local clusters. In 11 out of the 18 considered cases, the largest cluster contributes more than 50% of the total connectivity. Fracture strength variability can lead to multiple local clusters but may not significantly enhance total connectivity. A large injection rate and high viscosity, combined with low strength variability, result in maximum connectivity in Case 12.
- Fluid production and connectivity are positively correlated, though not equivalent. In low-permeability reservoirs, production is primarily determined by the total fracture length connected to the production well. Fracture clusters connected to the production wells can contribute immediately, while local clusters may enhance production over the long term.
- Injection rate, fluid viscosity, fracture orientation, and clustering effects have consistent positive correlations with total connectivity and fluid production. Heterogeneity exhibits a weak positive correlation with fluid production, while it has a moderate negative correlation with total connectivity.

## Data Availability Statement

The numerical simulation utilized in this study relies on the freely available multi-physics simulation framework MECHSYS, created by Dr. S.A. Galindo Torres. This software package can be accessed via the website <https://mechsys.nongnu.org/>.

## Acknowledgments

The research conducted in this project was funded by National Natural Science Foundation of China (Grant 42141009), the Key Research Program of the Institute of Geology and Geophysics, CAS (Grant IGGCAS-202201), the National Key Research and Development Program of China (Grant 2019YFA0708704), the Youth Innovation Promotion Association Foundation of the Chinese Academy of Sciences (Grant 2023073), and the Second Tibetan Plateau Scientific Expedition and Research Program (Grant 2019QZKK0904). The authors would like to extend their appreciation to Dr. Xiang Li from Ennosoft and Prof. Dongxiao Zhang from the Eastern Institute of Technology for providing the UNCONG simulator, which was utilized for simulating two-phase flow in complex fracture-matrix systems (X. Li et al., 2015). The simulation was carried out with the support of the High-Performance Computing Center of Tsinghua University.

## References

- Alghalandis, Y. F., Dowd, P. A., & Xu, C. (2015). Connectivity field: A measure for characterising fracture networks. *Mathematical Geosciences*, 47(1), 63–83. <https://doi.org/10.1007/s11004-014-9520-7>
- Bahorich, B., Olson, J. E., & Holder, J. (2012). Examining the effect of cemented natural fractures on hydraulic fracture propagation in hydrostone block experiments. In *SPE Annual Technical Conference and Exhibition* (pp. SPE–160197).
- Barati, R., & Liang, J.-T. (2014). A review of fracturing fluid systems used for hydraulic fracturing of oil and gas wells. *Journal of Applied Polymer Science*, 131(16), 40735. <https://doi.org/10.1002/app.40735>
- Barton, C., & Hsieh, P. A. (1989). Physical and hydrologic-flow properties of fractures. In *28th International Geological Congress Field Trip Guidebook* (Vol. 385, p. 36).
- Barton, C. A., Zoback, M. D., & Moos, D. (1995). Fluid flow along potentially active faults in crystalline rock. *Geology*, 23(8), 683–686. [https://doi.org/10.1130/0091-7613\(1995\)023<0683:ffapaf>2.3.co;2](https://doi.org/10.1130/0091-7613(1995)023<0683:ffapaf>2.3.co;2)
- Berkowitz, B., Bour, O., Davy, P., & Odling, N. (2000). Scaling of fracture connectivity in geological formations. *Geophysical Research Letters*, 27(14), 2061–2064. <https://doi.org/10.1029/1999gl011241>
- Bing, H., Mian, C., Zhimeng, L., Yonghui, W., & Ce, D. (2014). Propagation area evaluation of hydraulic fracture networks in shale gas reservoirs. *Petroleum Exploration and Development*, 41(6), 833–838. [https://doi.org/10.1016/s1876-3804\(14\)60101-4](https://doi.org/10.1016/s1876-3804(14)60101-4)
- Bour, O., & Davy, P. (1997). Connectivity of random fault networks following a power law fault length distribution. *Water Resources Research*, 33(7), 1567–1583. <https://doi.org/10.1029/96wr00433>
- Chen, H., Meng, X., Niu, F., Tang, Y., Yin, C., & Wu, F. (2018). Microseismic monitoring of stimulating shale gas reservoir in SW China: 2. Spatial clustering controlled by the preexisting faults and fractures. *Journal of Geophysical Research: Solid Earth*, 123(2), 1659–1672. <https://doi.org/10.1002/2017jb014491>
- Chen, Z., Elsworth, D., & Wang, M. (2020). Does low-viscosity fracturing fluid always create complex fractures? *Journal of Geophysical Research: Solid Earth*, 125(9), e2020JB020332. <https://doi.org/10.1029/2020jb020332>
- Chen, Z., Jin, X., & Wang, M. (2018). A new thermo-mechanical coupled DEM model with non-spherical grains for thermally induced damage of rocks. *Journal of the Mechanics and Physics of Solids*, 116, 54–69. <https://doi.org/10.1016/j.jmps.2018.03.023>
- Chen, Z., Shu, C., Yang, L., Zhao, X., & Liu, N. (2020). Immersed boundary–simplified thermal lattice Boltzmann method for incompressible thermal flows. *Physics of Fluids*, 32(1), 013605. <https://doi.org/10.1063/1.5138711>
- Chen, Z., & Wang, M. (2017). Pore-scale modeling of hydromechanical coupled mechanics in hydrofracturing process. *Journal of Geophysical Research: Solid Earth*, 122(5), 3410–3429. <https://doi.org/10.1002/2017jb013989>
- Chen, Z., & Wang, M. (2020). An improved immersed moving boundary for hydrodynamic force calculation in lattice Boltzmann method. *International Journal for Numerical Methods in Engineering*, 121(20), 4493–4508. <https://doi.org/10.1002/nme.6444>
- Chen, Z., Yang, Z., & Wang, M. (2018). Hydro-mechanical coupled mechanisms of hydraulic fracture propagation in rocks with cemented natural fractures. *Journal of Petroleum Science and Engineering*, 163, 421–434. <https://doi.org/10.1016/j.petrol.2017.12.092>
- Chuprakov, D. A., Akulich, A. V., Siebrits, E., & Thiercelin, M. (2011). Hydraulic-fracture propagation in a naturally fractured reservoir. *SPE Production & Operations*, 26(01), 88–97. <https://doi.org/10.2118/128715-pa>
- Cormen, T. H., Leiserson, C. E., Rivest, R. L., & Stein, C. (2022). *Introduction to algorithms*. MIT Press.
- Dehghan, A. N. (2020). An experimental investigation into the influence of pre-existing natural fracture on the behavior and length of propagating hydraulic fracture. *Engineering Fracture Mechanics*, 240, 107330. <https://doi.org/10.1016/j.engfracmech.2020.107330>
- Duan, K., Kwok, C. Y., Wu, W., & Jing, L. (2018). Dem modeling of hydraulic fracturing in permeable rock: Influence of viscosity, injection rate and in situ states. *Acta Geotechnica*, 13(5), 1187–1202. <https://doi.org/10.1007/s11440-018-0627-8>
- Fisher, M. K., Wright, C. A., Davidson, B. M., Goodwin, A., Fielder, E., Buckler, W., et al. (2002). Integrating fracture mapping technologies to optimize stimulations in the Barnett Shale. In *SPE Annual Technical Conference and Exhibition*.
- Gabriel, A.-A., Garagash, D. I., Palgunadi, K. H., & Mai, P. M. (2024). Fault size–dependent fracture energy explains multiscale seismicity and cascading earthquakes. *Science*, 385(6707), eadj9587. <https://doi.org/10.1126/science.adj9587>
- Galindo-Torres, S. A., Pedroso, D., Williams, D., & Li, L. (2012). Breaking processes in three-dimensional bonded granular materials with general shapes. *Computer Physics Communications*, 183(2), 266–277. <https://doi.org/10.1016/j.cpc.2011.10.001>
- Gandossi, L., & Von Estorff, U. (2013). *An overview of hydraulic fracturing and other formation stimulation technologies for shale gas production* (p. 26347). European Commission's Joint Research Centre Technical Reports.
- Geertsma, J., & De Klerk, F. (1969). A rapid method of predicting width and extent of hydraulically induced fractures. *Journal of Petroleum Technology*, 21(12), 1571–1581. <https://doi.org/10.2118/2458-pa>
- Haimson, B., & Fairhurst, C. (1969). In-situ stress determination at great depth by means of hydraulic fracturing. In *ARMA US Rock Mechanics/ Geomechanics Symposium* (pp. ARMA–69).
- Khrstianovic, S., & Zheltov, Y. P. (1955). Formation of vertical fractures by means of highly viscous liquid. In *World Petroleum Congress Proceedings* (pp. 579–586).
- Kolawole, O., & Ispas, I. (2020). Interaction between hydraulic fractures and natural fractures: Current status and prospective directions. *Journal of Petroleum Exploration and Production Technology*, 10(4), 1613–1634. <https://doi.org/10.1007/s13202-019-00778-3>
- Krzaczek, M., Nitka, M., & Tejchman, J. (2021). Effect of gas content in macropores on hydraulic fracturing in rocks using a fully coupled DEM/CFD approach. *International Journal for Numerical and Analytical Methods in Geomechanics*, 45(2), 234–264. <https://doi.org/10.1002/nag.3160>
- Kumari, W., Ranjith, P., Perera, M., Li, X., Li, L., Chen, B., et al. (2018). Hydraulic fracturing under high temperature and pressure conditions with micro CT applications: Geothermal energy from hot dry rocks. *Fuel*, 230, 138–154. <https://doi.org/10.1016/j.fuel.2018.05.040>
- Lakirouhani, A., Detournay, E., & Bungler, A. (2016). A reassessment of in situ stress determination by hydraulic fracturing. *Geophysical Journal International*, 205(3), 1859–1873. <https://doi.org/10.1093/gji/ggw132>

- Laubach, S., Reed, R., Olson, J., Lander, R., & Bonnell, L. (2004). Coevolution of crack-seal texture and fracture porosity in sedimentary rocks: Cathodoluminescence observations of regional fractures. *Journal of Structural Geology*, 26(5), 967–982. <https://doi.org/10.1016/j.jsg.2003.08.019>
- Laubach, S. E. (2003). Practical approaches to identifying sealed and open fractures. *AAPG Bulletin*, 87(4), 561–579. <https://doi.org/10.1306/11060201106>
- Laubach, S. E., & Ward, M. E. (2006). Diagenesis in porosity evolution of opening-mode fractures, Middle Triassic to Lower Jurassic la Boca Formation, NE Mexico. *Tectonophysics*, 419(1–4), 75–97. <https://doi.org/10.1016/j.tecto.2006.03.020>
- Lei, Q., Latham, J.-P., & Tsang, C.-F. (2017). The use of discrete fracture networks for modelling coupled geomechanical and hydrological behaviour of fractured rocks. *Computers and Geotechnics*, 85, 151–176. <https://doi.org/10.1016/j.compgeo.2016.12.024>
- Li, S., Zhang, D., & Li, X. (2017). A new approach to the modeling of hydraulic-fracturing treatments in naturally fractured reservoirs. *SPE Journal*, 22(04), 1064–1081. <https://doi.org/10.2118/181828-pa>
- Li, X., Zhang, D., & Li, S. (2015). A multi-continuum multiple flow mechanism simulator for unconventional oil and gas recovery. *Journal of Natural Gas Science and Engineering*, 26, 652–669. <https://doi.org/10.1016/j.jngse.2015.07.005>
- Li, Y., Hu, W., Zhang, Z., Zhang, Z., Shang, Y., Han, L., & Wei, S. (2021). Numerical simulation of hydraulic fracturing process in a naturally fractured reservoir based on a discrete fracture network model. *Journal of Structural Geology*, 147, 104331. <https://doi.org/10.1016/j.jsg.2021.104331>
- Liu, P., Ju, Y., Gao, F., Ranjith, P. G., & Zhang, Q. (2018). CT identification and fractal characterization of 3-D propagation and distribution of hydrofracturing cracks in low-permeability heterogeneous rocks. *Journal of Geophysical Research: Solid Earth*, 123(3), 2156–2173. <https://doi.org/10.1002/2017jb015048>
- Liu, P., Ju, Y., Ranjith, P. G., Zheng, Z., & Chen, J. (2016). Experimental investigation of the effects of heterogeneity and geostress difference on the 3D growth and distribution of hydrofracturing cracks in unconventional reservoir rocks. *Journal of Natural Gas Science and Engineering*, 35, 541–554. <https://doi.org/10.1016/j.jngse.2016.08.071>
- Marder, M., Chen, C.-H., & Patzek, T. (2015). Simple models of the hydrofracture process. *Physical Review E*, 92(6), 062408. <https://doi.org/10.1103/physreve.92.062408>
- Marsden, H., Basu, S., Striolo, A., & MacGregor, M. (2022). Advances of nanotechnologies for hydraulic fracturing of coal seam gas reservoirs: Potential applications and some limitations in Australia. *International Journal of Coal Science & Technology*, 9(1), 27. <https://doi.org/10.1007/s40789-022-00497-x>
- Mayerhofer, M. J., Lonon, E., Warpinski, N. R., Cipolla, C. L., Walsler, D. W., Rightmire, C. M., et al. (2010). What is stimulated reservoir volume? *SPE Production & Operations*, 25(01), 89–98. <https://doi.org/10.2118/119890-pa>
- Morgan, S., Li, B., & Einstein, H. (2017). Effect of injection rate on hydraulic fracturing of Opalinus clay shale. In *51st US Rock Mechanics/ Geomechanics Symposium*.
- Noble, D., & Torczynski, J. (1998). A lattice-Boltzmann method for partially saturated computational cells. *International Journal of Modern Physics C*, 9(08), 1189–1201. <https://doi.org/10.1142/s0129183198001084>
- Nordgren, R. (1972). Propagation of a vertical hydraulic fracture. *Society of Petroleum Engineers Journal*, 12(04), 306–314. <https://doi.org/10.2118/3009-pa>
- Olson, J. E., Bahorich, B., & Holder, J. (2012). Examining hydraulic fracture-natural fracture interaction in hydrostone block experiments. In *SPE Hydraulic Fracturing Technology Conference and Exhibition* (pp. SPE-152618).
- Perkins, T., & Kern, L. R. (1961). Widths of hydraulic fractures. *Journal of Petroleum Technology*, 13(09), 937–949. <https://doi.org/10.2118/89-pa>
- Pruess, K. (2006). Enhanced geothermal systems (EGS) using CO<sub>2</sub> as working fluid—A novel approach for generating renewable energy with simultaneous sequestration of carbon. *Geothermics*, 35(4), 351–367. <https://doi.org/10.1016/j.geothermics.2006.08.002>
- Qi, S., Wu, F., Yan, F., & Lan, H. (2004). Mechanism of deep cracks in the left bank slope of Jinping first stage hydropower station. *Engineering Geology*, 73(1–2), 129–144. <https://doi.org/10.1016/j.enggeo.2003.12.005>
- Rateman, K. T., Farrell, H. E., Mora, O. S., Janssen, A. L., Gomez, G. A., Busetti, S., et al. (2018). Sampling a stimulated rock volume: An Eagle Ford example. *SPE Reservoir Evaluation & Engineering*, 21(04), 927–941. <https://doi.org/10.2118/191375-pa>
- Riffault, J., Dempsey, D., Karra, S., & Archer, R. (2018). Microseismicity cloud can be substantially larger than the associated stimulated fracture volume: The case of the Parana Enhanced Geothermal System. *Journal of Geophysical Research: Solid Earth*, 123(8), 6845–6870. <https://doi.org/10.1029/2017jb015299>
- Sanderson, D. J., & Nixon, C. W. (2015). The use of topology in fracture network characterization. *Journal of Structural Geology*, 72, 55–66. <https://doi.org/10.1016/j.jsg.2015.01.005>
- Shimizu, H., Murata, S., & Ishida, T. (2011). The distinct element analysis for hydraulic fracturing in hard rock considering fluid viscosity and particle size distribution. *International Journal of Rock Mechanics and Mining Sciences*, 48(5), 712–727. <https://doi.org/10.1016/j.ijrmms.2011.04.013>
- Taleghani, A. D., & Olson, J. E. (2014). How natural fractures could affect hydraulic-fracture geometry. *SPE Journal*, 19(01), 161–171. <https://doi.org/10.2118/167608-pa>
- Ukar, E., & Laubach, S. E. (2016). Syn- and postkinematic cement textures in fractured carbonate rocks: Insights from advanced cathodoluminescence imaging. *Tectonophysics*, 690, 190–205. <https://doi.org/10.1016/j.tecto.2016.05.001>
- Van Mier, J. G., van Vliet, M. R., & Wang, T. K. (2002). Fracture mechanisms in particle composites: Statistical aspects in lattice type analysis. *Mechanics of Materials*, 34(11), 705–724. [https://doi.org/10.1016/s0167-6636\(02\)00170-9](https://doi.org/10.1016/s0167-6636(02)00170-9)
- Wang, S., Zhou, J., Zhang, L., Han, Z., & Kong, Y. (2024). Numerical insight into hydraulic fracture propagation in hot dry rock with complex natural fracture networks via fluid-solid coupling grain-based modeling. *Energy*, 295, 131060. <https://doi.org/10.1016/j.energy.2024.131060>
- Wu, K., & Olson, J. E. (2016). Numerical investigation of complex hydraulic-fracture development in naturally fractured reservoirs. *SPE Production & Operations*, 31(04), 300–309. <https://doi.org/10.2118/173326-pa>
- Yaobin, S., Weiyong, L., Changchun, H., & Erhu, B. (2020). Numerical simulation of the influence of natural fractures on hydraulic fracture propagation. *Geofluids*, 2020(1), 8878548. <https://doi.org/10.1155/2020/8878548>
- Ye, Z., Fan, X., Zhang, J., Sheng, J., Chen, Y., Fan, Q., & Qin, H. (2021). Evaluation of connectivity characteristics on the permeability of two-dimensional fracture networks using geological entropy. *Water Resources Research*, 57(10), e2020WR029289. <https://doi.org/10.1029/2020wr029289>
- Zeng, Q., & Yao, J. (2016). Numerical simulation of fracture network generation in naturally fractured reservoirs. *Journal of Natural Gas Science and Engineering*, 30, 430–443. <https://doi.org/10.1016/j.jngse.2016.02.047>

- Zhou, C., Qian, J.-G., Yin, Z.-Y., Liu, Y.-J., & Du, Z.-B. (2023). Effect of particle shape and bedding angle on suffusion in gap-graded granular soils by coupled CFD-DEM method. *International Journal for Numerical and Analytical Methods in Geomechanics*, 47(8), 1373–1398. <https://doi.org/10.1002/nag.3519>
- Zhu, W., Chen, Z., He, X., Tian, Z., & Wang, M. (2023). Numerical investigation of influential factors in hydraulic fracturing processes using coupled discrete element-lattice Boltzmann method. *Journal of Geophysical Research: Solid Earth*, 128(9), e2023JB027292. <https://doi.org/10.1029/2023jb027292>
- Zhu, W., He, X., Khirevich, S., & Patzek, T. W. (2022). Fracture sealing and its impact on the percolation of subsurface fracture networks. *Journal of Petroleum Science and Engineering*, 218, 111023. <https://doi.org/10.1016/j.petrol.2022.111023>
- Zhu, W., He, X., Li, Y., Lei, G., Santoso, R., & Wang, M. (2022). Impacts of fracture properties on the formation and development of stimulated reservoir volume: A global sensitivity analysis. *Journal of Petroleum Science and Engineering*, 217, 110852. <https://doi.org/10.1016/j.petrol.2022.110852>
- Zhu, W., He, X., Patzek, T. W., Cheng, Z., Hoteit, H., Elsworth, D., et al. (2024). A novel connectivity metric of identified multi-cluster fracture networks in permeable formations. *Geophysical Research Letters*, 51(14), e2024GL109569. <https://doi.org/10.1029/2024gl109569>
- Zhu, W., He, X., Santoso, R. K., Lei, G., Patzek, T. W., & Wang, M. (2022). Enhancing fracture network characterization: A data-driven, outcrop-based analysis. *Computers and Geotechnics*, 152, 104997. <https://doi.org/10.1016/j.compgeo.2022.104997>
- Zhu, W., Khirevich, S., & Patzek, T. (2018). Percolation properties of stochastic fracture networks in 2D and outcrop fracture maps. In *80th EAGE Conference and Exhibition 2018* (Vol. 2018, pp. 1–5).
- Zhu, W., Khirevich, S., & Patzek, T. W. (2021). Impact of fracture geometry and topology on the connectivity and flow properties of stochastic fracture networks. *Water Resources Research*, 57(7), e2020WR028652. <https://doi.org/10.1029/2020wr028652>
- Zhu, W., Khirevich, S., & Patzek, T. W. (2022). HatchFrac: A fast open-source DFN modeling software. *Computers and Geotechnics*, 150, 104917. <https://doi.org/10.1016/j.compgeo.2022.104917>
- Zhu, W., Lei, G., He, X., Yang, Y., Santoso, R. K., & Wang, M. (2022). Can we infer the percolation status of 3D fractured media from 2D outcrops? *Engineering Geology*, 302, 106648. <https://doi.org/10.1016/j.enggeo.2022.106648>
- Zoback, M. D., & Gorelick, S. M. (2012). Earthquake triggering and large-scale geologic storage of carbon dioxide. *PNAS*, 109(26), 10164–10168. <https://doi.org/10.1073/pnas.1202473109>
- Zoback, M. D., & Haimson, B. C. (1982). Status of the hydraulic fracturing method for in-situ stress measurements. In *ARMA US Rock Mechanics/ Geomechanics Symposium* (pp. ARMA–82).

## References From the Supporting Information

- Bonnet, E., Bour, O., Odling, N. E., Davy, P., Main, I., Cowie, P., & Berkowitz, B. (2001). Scaling of fracture systems in geological media. *Reviews of Geophysics*, 39(3), 347–383. <https://doi.org/10.1029/1999rg000074>
- Buckingham, E. (1915). The principle of similitude. *Nature*, 96(2406), 396–397. <https://doi.org/10.1038/096396d0>
- Darcel, C., Bour, O., Davy, P., & De Dreuzy, J. (2003). Connectivity properties of two-dimensional fracture networks with stochastic fractal correlation. *Water Resources Research*, 39(10), 1272. <https://doi.org/10.1029/2002wr001628>
- Galindo-Torres, S. A. (2013). A coupled discrete element lattice Boltzmann method for the simulation of fluid–solid interaction with particles of general shapes. *Computer Methods in Applied Mechanics and Engineering*, 265, 107–119. <https://doi.org/10.1016/j.cma.2013.06.004>
- Gong, F., Zhang, L., & Wang, S. (2019). Loading rate effect of rock material with the direct tensile and three Brazilian disc tests. *Advances in Civil Engineering*, 2019(1), 6260351. <https://doi.org/10.1155/2019/6260351>
- Kemeny, J., & Post, R. (2003). Estimating three-dimensional rock discontinuity orientation from digital images of fracture traces. *Computers & Geosciences*, 29(1), 65–77. [https://doi.org/10.1016/s0098-3004\(02\)00106-1](https://doi.org/10.1016/s0098-3004(02)00106-1)
- Meakin, P. (1991). Invasion percolation on substrates with correlated disorder. *Physica A*, 173(3), 305–324. [https://doi.org/10.1016/0378-4371\(91\)90366-k](https://doi.org/10.1016/0378-4371(91)90366-k)
- Segall, P., & Pollard, D. D. (1983). Joint formation in granitic rock of the Sierra Nevada. *Geological Society of America Bulletin*, 94(5), 563–575. [https://doi.org/10.1130/0016-7606\(1983\)94<563:jfigro>2.0.co;2](https://doi.org/10.1130/0016-7606(1983)94<563:jfigro>2.0.co;2)
- Song, J.-J., Lee, C.-I., & Seto, M. (2001). Stability analysis of rock blocks around a tunnel using a statistical joint modeling technique. *Tunnelling and Underground Space Technology*, 16(4), 341–351. [https://doi.org/10.1016/s0886-7798\(01\)00063-3](https://doi.org/10.1016/s0886-7798(01)00063-3)
- Strack, O. E., & Cook, B. K. (2007). Three-dimensional immersed boundary conditions for moving solids in the lattice-Boltzmann method. *International Journal for Numerical Methods in Fluids*, 55(2), 103–125. <https://doi.org/10.1002/flid.1437>
- Whitaker, A. E., & Engelder, T. (2005). Characterizing stress fields in the upper crust using joint orientation distributions. *Journal of Structural Geology*, 27(10), 1778–1787. <https://doi.org/10.1016/j.jsg.2005.05.016>